Journal of Molecular Liquids 320 (2020) 114347

Contents lists available at ScienceDirect

Journal of Molecular Liquids

journal homepage: www.elsevier.com/locate/molliq

Correlated counterion effects on the solvation of proteins by ionic liquids

Vinicius Piccoli, Leandro Martínez *

Institute of Chemistry and Center for Computing in Engineering & Science, University of Campinas, Campinas, SP, Brazil

ARTICLE INFO

Article history:
Received 8 June 2020
Received in revised form 28 August 2020
Accepted 15 September 2020
Available online 28 September 2020

Keywords:
Ionic liquids
Proteins
Solvation
Kirkwood-buff
Distribution functions
Simulations

ABSTRACT

Ionic liquids are versatile compounds for biotechnological applications. However, even the chemical systems composed only of the IL, water, and of the biomolecules display complex interactions that are not reducible in terms of the possible pairs of components. Here, we illustrate this complexity and provide a molecular understanding of cooperative solvation effects by studying Ubiquitin in solutions of the four ionic liquids formed by the combinations of the cations 1-Ethyl-3-methylimidazolium (EMIM), and 1-Butyl-3-methylimidazolium (BMIM), and of the anions Tetrafluoroborate (BF4), and Dicyanamide (DCA), using computer simulations. The structure and thermodynamics of the protein-IL interactions were evaluated by means of minimum-distance distribution functions (MDDFs) and the Kirkwood-Buff (KB) theory of solvation using the ComplexMixtures (http://m3g.iqm.unicamp.br/ComplexMixtures) software. The cooperativity of the interactions of the ions with the protein stems from the necessary electrical neutrality of the bulk solution. Specifically, the counterions' KB integrals are identical despite their contrasting interactions with the protein surface. Therefore, varying the hydrophobicity of the cation or the chemical nature of the anion implies different distributions of the corresponding counterions in the solution. The DCA anion, by forming hydrogen bonds to the protein surface, can drive the cations to the proximity of the protein surface. This effect is localized in the first two or three solvation shells of the protein. Direct correlations of the positions of the ions by alternating density augmentations can be observed at specific protein surface sites. At the same time, the protein can become preferentially hydrated by increasing the hydrophobicity of the cation and its concentration, independently of the strength of the interactions of the anion with the protein surface. In summary, cooperative ion effects determine the strength of the interactions of each component of the solution with the protein and the final solubility, and stability, of the biomolecules. Tuning the properties of ILs for specific applications rely on the understanding of these many-component effects.

1. Introduction

Ionic liquids are compounds with low melting points (usually under 100 °C) having a number interesting physicochemical properties: low vapor pressure, high viscosity, thermal stability, and solvation ability, for example [1–3]. They are used as solvents in electrolytic devices [4], catalysis [5], organic synthesis [6], or for separation and purification [7].

Ionic liquids have attracted interest in biotechnological systems - notably in protein conservation [8], separation [8,9], crystallization [8–11], and catalysis [12–15]. Ionic liquids are being studied, frequently as solvents, for various proteins, like keratins [16,17], collagens [18], plant proteins [19], and silks [20].

To exert function, most proteins need to display specific tridimensional shapes. In biological and industrial applications, proteins are found in solutions crowded with other molecules that can interfere in their conformational equilibrium [21,22]. Osmolytes are small organic molecules that are present in biological solutions, or are added to chemical systems, to control the stability of the active protein structure. Common osmolytes are polyols (glycerol, sorbitol trehalose, etc.), amino acids, methylamines, and urea [21]. Osmolytes are regularly investigated due to their influence in protein folding [23,24]. The stabilization/destabilization effect of an osmolyte on a protein conformation will depend if the osmolyte interacts favorably or not with the protein surface relative to the solution, leading to preferential stabilization by preferential hydration or destabilization by dehydration [25,26].

Ions can also interfere in the protein structure. The influence that the ions have on protein structures is summarized by the Hofmeister series, which consists of a classification of ionic species in order of their ability to salt-out or salt-in proteins [27]. An ionic liquid is intrinsically formed by two ions, such that it is possible to modulate the stability and solubility of a protein by varying one or other ion, or both [11,25,28,29]. The understanding of interactions of ionic liquid ions with proteins, and the role of ion exchange, is important for the design of ionic liquids with possible applications in biotechnology [30].

* Corresponding author at: Institute of Chemistry, University of Campinas, 13083-970 Campinas, SP, Brazil.
E-mail addresses: leandro@iqm.unicamp.br,
URL: http://m3g.iqm.unicamp.br (L. Martínez).

https://doi.org/10.1016/j.molliq.2020.114347
0167-7322/

The cation of an ionic liquid is, usually, an organic molecule (like imidazolium, alkylammonium, and pyrrolidinium) [31]. The anion might be organic (like acetate) or inorganic (Chloride, Bromide, etc.) [32]. The ionic liquid chemical properties are influenced by the cation and by the anion [33–35]. A hydrophobic cation might interact via dispersion forces with a solute, while a polar anion might be able to establish hydrogen bonds or polar interactions with the solute [31]. Specific cation/anion combinations can be used to tune the ionic liquid properties [11,36,37].

The interactions of all species in a system composed of proteins, water, and ionic liquids are not simple to understand [3,38,39]. The interaction between solvent molecules and macromolecules can be analyzed via the excess or the deficit, around the solute, of the solvent molecules relative to their bulk concentrations [21]. Microscopic and macroscopic properties can be connected by means of the Kirkwood-Buff (KB) theory of solutions [39–42]. Following KB theory, distribution functions describing the density of the components of the solution in space can be used to compute Kirkwood-Buff integrals. These integrals are a measure of effective molar volume changes of the solvent implied by the presence of the solute of interest, a protein for example, resulting from local density variations around the solute. These density variations can be studied by means of distribution functions (DFs). DFs can be computed from Molecular Dynamics (MD) simulations, and are particularly interesting if able to provide a clear picture of solute-solvent interactions, something that is not trivial for molecules of complex shapes, and with surfaces with heterogeneous chemical nature.

We have been exploring the use of Minimum-Distance Distributions Functions (MDDFs) to study the interactions of complex-shaped solutes with solvents of variable chemical nature [43,44]. In MDDFs, the distance-metric defined between the solute and the solvent is the shortest distance between any solute and solvent atoms, for each solvent molecule. Therefore, a density augmentation at a given shortest-distance is directly associated with specific bonds or other favorable interactions, and the density profiles obtained are very easy to interpret in terms of the intermolecular interactions of the solvent at the surface of the solute. MDDFs, furthermore, are practical for computing preferential interaction parameters through KB solution theory, to obtain thermodynamic properties of the solution [43,44].

Here, we perform molecular dynamics simulations of Ubiquitin in solutions of the four ionic liquids formed by combination of the cations 1-Ethyl-3-methylimidazolium (EMIM), and 1-Butyl-3-methylimidazolium (BMIM), and of the anions Tetrafluoroborate (BF4), and Dicyanamide (DCA), at various concentrations. By varying the aliphatic chain of the cation we are able to study the effect of the hydrophobic character of this ion in the solvent structure. At the same time, DCA is a strong hydrogen-bond acceptor, which is not the case of the BF4 anion. Thus, different properties of the ILs are probed by scanning the combinations of these ions.

We study the solvation structures using MDDFs, which provide a rich and detailed view of solute-solvent interactions for complex systems with a solvent-shell, intuitive, perspective. The decomposition of the MDDFs into the contributions of each solvent and solute chemical group allows a detailed description of the protein-ion and protein-water interactions. Additionally, from the MDDFs we compute Kirkwood-Buff integrals and preferential interaction parameters for water and for the ionic liquid components. Some fundamental questions associated with Protein/IL interactions were addressed: 1) Solvation structures suggest that the ILs are stabilizers or denaturing agents? 2) How is the interplay between the two ions? 3) Is the protein preferentially hydrated or dehydrated? 4) The preferential binding of water or the IL is concentration-dependent? We show that the ILs presented can act both as stabilizers or denaturing agents in a concentration-dependent manner. There is a complex and interesting correlation between the solvation of the protein by the two ions which, while interacting very differently with the protein surface, result to be identically preferentially bound to the protein because of the required electroneutrality of the solution. However, these counterion correlations are mostly localized in the initial solvation shells of the protein. Due to these correlations, it is not possible to decompose the role of each ion in the thermodynamic solvation effects, and the design of ILs depends on understanding the correlated counterion effects on protein solvation structures.

2. Methods

2.1. Minimum-distance distribution functions

The formalism and computational strategies to obtain distribution functions and preferential interaction parameters are described in this section. Previous publications provide complementary descriptions of these methods applied to other molecular systems [43,44]. Here we will study quaternary solutions containing the protein (species p), water (species$w$) and the ionic liquid formed by a cation (species c) and an anion (species a). The protein is considered to be at infinite dilution. The molar concentrations of water and the ionic liquid ions are $\rho_w$and $\rho_c = \rho_a$, respectively. The distribution of one of the cation, for example, around the protein can be described by the average number density $n_c(r)$ of cation ions relative to the density of an ideal-gas distribution, $n_c^*(r)$,

$$g_{pc}(r) = \frac{n_c(r)}{n_c^*(r)} \tag{1}$$

where r is the distance between the protein and the cation ion. If a single reference of coordinates is used for the protein and for the cation, $g_{pc}(r)$ is a radial distribution function. In particular, if the center of mass of the solvent is used as the reference coordinate of the distributions, $n_c^*(r)$ is constant and equal to the molar density of the solvent, such that $g_{pc}(r) = \frac{n_c(r)}{\rho_c}$, which is the most common definition of a radial distribution function. The interpretation of radial distribution functions in terms of direct molecular interactions might be cumbersome if the solutes and solvents have molecular structures that are far from spherical, and are dependent on the choice of the reference solute and solvent atoms [45–49]. Alternate definitions for the distance between the solute and the solvent are more practical and easy to interpret if the molecules involved have complex shapes [50–52]. Here, we use the minimum distance between any atom of the solvent and any atom of the protein [43,53], which defines a minimum-distance distribution function (MDDF).

For MDDFs, the ideal-gas density of the solvent, $n_c^*(r)$, is not constant, even given the fact that no intermolecular interactions are present. This is because the minimum-distance count is such that at every r what is being computed is the density of solvent molecules that have *one of its atoms* at a distance r from the solute, and no atom closer than r. In particular, this is dependent on the number of atoms of the solvent and on the shape of the solute and solvent molecules. Therefore defining a reference state for MDDFs is tricky. One alternative is to simulate random configurations of the solvent around the solute, ignoring solute-solvent interactions. With this choice, the MDDFs are associated with the potential of mean-force of organization of the solvent around the solute [43]. Most importantly, MDDFs are very natural to interpret in terms of solute-solvent interactions and can be used to obtain KB integrals and preferential interaction parameters [43,44].

As the real $[n_c(r)]$ and ideal $[n_c^*(r)]$ number densities of minimum-distances between solute and solvent vary with the distance in MDDFs, the equation for KB integrals has to be generalized to

$$G_{pc} = \frac{1}{\rho_c}\int_0^\infty \left[n_c(r) - n_c^*(r)\right] S(r) dr \tag{2}$$

where $S(r)$ is the surface area element at distance r. For a minimum-distance count $S(r)$ is dependent on the shape of the solute [43]. This equation reduces to the most common radial representation of KB integrals by using $n_c^*(r) = \rho_c$and $S(r) = 4\pi r^2$.

In practice, computing G_{pc} from a MD simulation consists in counting the number of solvent molecules within a distance R of the solute, with R large enough such that the solute does not affect the solution structure above this limit. Eq. (2) then reduces to

$$G_{pc}(R) = \frac{1}{\rho_c}\left[N_{pc}(R) - N^*_{pc}(R)\right] \quad (3)$$

where $N_{pc}(R)$ is the number of protein and solvent minimum-distances smaller than R in the solution and $N^*_{pc}(R)$ is the number of equivalent distances within R in the absence of solute-solvent interactions. $N^*_{pc}(R)$ can be obtained from a conventional simulation, while $n^*_c(r)$ depends on simulating a random distribution solvent molecules around the protein [43].

The "protein domain" is the region around the protein where protein-solvent interactions cannot be neglected ($r < R$). The KB integrals, as defined in Eqs. (2) and (3), are the excess volume occupied by the cosolvent in the protein domain, relative to the volume it would occupy if there were no solute-solvent interactions [21,54,55]. If the solvent interactions with the solute are favorable, it accumulates on the protein domain and the KB integral becomes positive. If on the other side, the interactions of the solvent with the bulk solution are preferred, the solvent density in the protein domain is smaller than that in bulk, and the KB integral is negative. The detailed balance of solute-solvent and solvent-solvent interactions determines the final preferential binding or depletion of the solvent by the addition of the solute to the system.

The preferential solvation parameter is computed from the difference of KB integrals of solvent components and dictates which component is preferentially bound to the solute [21,42,56,57]. In our case, for example, the IL preferential binding relative to water is

$$\Gamma_{pc}(R) \approx \rho_c\left[G_{pc}(R) - G_{pw}(R)\right] \quad (4)$$

and consists of the number of cation (or anion, for the reasons that will be discussed below) molecules in excess or deficit in the protein domain, considering the cosolvent molecular volume in the bulk solution. Eqs. (1) to (4) for water relative to the cation provide the preferential hydration parameter, $\Gamma_{pw}(R)$,

$$\Gamma_{pw}(R) \approx \rho_w\left[G_{pw}(R) - G_{pc}(R)\right]. \quad (5)$$

A positive $\Gamma_{pc}(R)$ and a negative $\Gamma_{pw}(R)$ indicate that the protein is preferentially solvated by the cosolvent, thus, that the cosolvent molecules *accumulate* in the protein domain - the protein is effectively dehydrated. Alternatively, a positive preferential hydration parameter (and thus negative $\Gamma_{pc}(R)$) indicates that the cosolvent is *excluded* from the protein domain.

If $\Gamma_{pc}(R)$ is positive (and, thus, $\Gamma_{pw}(R)$ is negative), the IL interacts favorably with the protein and tends to stabilize structures with a greater solvent-accessible surface area. Since denatured protein states tend to have greater surface areas than functional states, cosolvents that preferentially bind to protein native states are, in most cases, denaturants [25,58–62]. Conversely, if the protein is preferentially hydrated ($\Gamma_{pw}(R)$ is positive), the solvent-accessible surface area tends to be minimized, and the protein folded state is stabilized. This is the rationale behind the stabilizing or destabilizing roles of osmolytes in general, under the assumption that the chemical nature of the protein surface does not change significantly upon denaturation [58,63,64].

Eqs. (4) and (5) are valid for three-component mixtures with neutral solutes. If the solute and solvent are charged, the accumulation or depletion of the solvent ions from the solute domain are dependent on the net charges of each molecule, and refined equations for the preferential binding coefficients are necessary [2,65–67]. If the solute is neutral, the KB integrals of cations and anions are expected to be equal to preserve the electroneutrality of the bulk solution, leading to the indistinguishability approach, in which all the ions are treated as a single component in the computation of preferential binding coefficients [42,59]. In this work, the protein is neutral, and we will show that the indistinguishable contributions of cations and anions to preferential binding coefficients is verified in practice, in such a way that Eqs. (4) and (5) can be used for the analysis of binding coefficients assuming a pseudo-three component mixture. In other words, KB integrals for cations, anions, or for both ions considered as a single component are equivalent, and preferential binding and hydration parameters can be computed from Eq. (5) without ambiguity. In practice, we report the preferential binding coefficients considering the ions as indistinguishable entities.

2.2. Molecular dynamics simulation

Molecular Dynamics (MD) simulations were performed for the crystal structure of human erythrocytic Ubiquitin (UBQ), PDB ID: 1UBQ [68]. The initial configurations were built using Packmol [69,70] containing the protein, water, and ionic liquid ions. No additional ions were used, and the protein Ubiquitin has no net charge, such that in all cases the neutrality of the simulation boxes was guaranteed by using the same number of cations and anions of each IL. The number of water molecules, IL ions, and resulting concentrations are shown in Table 1 and in Supp. Table S1.

Molecular dynamics simulations were performed using GROMACS. 2018.3 CUDA [71,72]. The simulations were performed as follows: (a) the potential energy was initially minimized for 50,000 Steepest-Descent steps while keeping all the protein coordinates fixed [73]; (b) Keeping the protein backbone fixed, 1 ns of thermal equilibration was performed in NVT conditions. (c) 5 ns MD were performed in isothermic-isobaric (NPT) conditions, also keeping the protein backbone fixed; (d) The restraints on the protein backbone were removed and a 1 ns simulation was performed with constant pressure and temperature; (e) Production simulations were 10 ns long and performed in the NPT ensemble. All equilibration and production simulations were performed at 1 bar and 300 K. The pressure was controlled using a Parrinello-Rahman barostat with 2.0 ps time constant [74,75] and the temperature was controlled using a modified-Berendsen velocity-rescaling thermostat [76,77] with a 0.1 ps period. A 10 Å cutoff was used for short-range interactions, and long-range electrostatic interactions were computed with the Particle-Mesh Ewald Summation method [78].

The OPLS-AA [76,79] force field was used for the protein, and the TIP3P [80] model was used for water. The OPLS-VSIL [81] force field was used for the ionic liquids. OPLS-VSIL is an improved force-field for ILs with a virtual charge site [82,83]. Its parametrization was performed to improve the accuracy in the computation of bulk IL properties such as the Henry constants, heat capacities, and vaporization enthalpies [84]. It has additionally been used, for example, for the study of organic reaction barriers in complex solvents [84,85] and anti-frost properties of IL-based gels [86].

For each system, 20 independent simulations were performed following the above protocol, starting from independently generated solvent boxes and random velocity distributions. By performing a set of short simulations instead of one long simulation for each system, we guarantee that UBQ structure retains its native conformation, and obtain sufficient sampling of the structure of the solvent. Therefore, we studied the solvation structure of the native state of the protein, without concurrent non-equilibrium denaturation effects in the time-scale of the simulations. The same protocol was used previously to study the solvation structures of other proteins in their native states [43,44,53]. The role of denatured states in the solvation thermodynamics of UBQ in ILs will be addressed in future studies.

A software to compute the MDDFs, KB integrals, and discriminate solute and solvent contributions is available as a Julia [87] package at http://m3g.iqm.unicamp.br/ComplexMixtures. The minimum-distance distribution functions were computed using a discretized version of

Table 1
Reference and effective concentrations of the IL solutions simulated, and Kirkwood-Buff integrals for all solvent components relative to the protein. Details on the construction of the systems are available in Supp. Table S1. Standard errors of the mean of at least 20 simulations are reported.

System	IL Concentration (reference/effective)/mol L^{-1}	KBI cation/L mol^{-1}	KBI anion/L mol^{-1}	KBI water/L mol^{-1}
EMIMDCA	0.5/0.465 ± 0.002	30.89 ± 2.64	31.40 ± 2.78	−9.32 ± 0.19
	1.0/0.960 ± 0.004	15.41 ± 2.26	17.43 ± 2.28	−10.58 ± 0.37
	1.5/1.493 ± 0.005	2.94 ± 1.65	3.66 ± 1.63	−9.51 ± 0.46
	2.0/2.024 ± 0.005	1.28 ± 1.38	1.58 ± 1.41	−10.09 ± 0.60
	2.5/2.597 ± 0.005	−5.85 ± 1.09	−5.75 ± 1.08	−6.86 ± 0.72
	3.0/3.151 ± 0.004	−5.49 ± 0.64	−5.50 ± 0.68	−7.18 ± 0.60
BMIMDCA	0.5/0.435 ± 0.003	66.56 ± 4.99	69.39 ± 4.67	−13.09 ± 0.38
	1.0/0.925 ± 0.006	36.23 ± 4.52	37.18 ± 4.21	−15.43 ± 0.76
	1.5/1.461 ± 0.007	12.98 ± 3.09	13.60 ± 2.88	−13.80 ± 0.98
	2.0/2.006 ± 0.008	3.08 ± 2.40	2.88 ± 2.23	−11.81 ± 1.30
	2.5/2.556 ± 0.008	−3.30 ± 1.80	−3.70 ± 1.70	−8.39 ± 1.53
	3.0/3.133 ± 0.005	−8.17 ± 0.81	−8.55 ± 0.80	−2.80 ± 1.15
	0.5/0.497 ± 0.001	0.32 ± 1.07	0.33 ± 0.90	−6.98 ± 0.08
EMIMBF4	1.0/1.021 ± 0.002	−2.99 ± 0.77	−3.22 ± 0.70	−7.06 ± 0.13
	1.5/1.569 ± 0.002	−3.98 ± 0.70	−3.99 ± 0.65	−7.17 ± 0.21
	2.0/2.152 ± 0.003	−6.07 ± 0.58	−6.14 ± 0.57	−6.55 ± 0.28
	2.5/2.768 ± 0.003	−7.18 ± 0.47	−7.31 ± 0.46	−5.75 ± 0.34
	3.0/3.419 ± 0.004	−8.51 ± 0.41	−8.57 ± 0.40	−3.95 ± 0.44
BMIMBF4	0.5/0.492 ± 0.002	5.01 ± 1.59	4.30 ± 1.34	−7.57 ± 0.14
	1.0/1.008 ± 0.002	−0.23 ± 1.10	−0.15 ± 0.96	−7.89 ± 0.23
	1.5/1.553 ± 0.004	−1.88 ± 1.20	−2.10 ± 1.06	−8.21 ± 0.44
	2.0/2.146 ± 0.004	−8.83 ± 1.06	−8.71 ± 0.96	−4.80 ± 0.66
	2.5/2.751 ± 0.004	−9.68 ± 0.72	−9.71 ± 0.69	−2.87 ± 0.73
	3.0/3.380 ± 0.003	−9.88 ± 0.48	−10.1 ± 0.46	0.10 ± 0.87

Eq. (1) in which the density was computed from the average number of minimum-distances at each 0.1 Å bin. The KB integrals and preferential interaction parameters were computed according to Eqs. (3) and (4), and the preferential hydration parameter according to Eq. (5). We used $R = 20$ Å, distance above which MDDFs were converged for practical purposes. The bulk concentrations of ionic liquids in Table 1 were computed from the simulations at distances $r > 20$ Å. The computation of the effective bulk concentrations from the simulations is necessary because the accumulation of the ILs in the protein domain can lead to significant variation of the number of IL molecules in the bulk solution, in particular for the most dilute solutions. In all figures, the data reported are averages of the 20 simulations performed for each system, and the standard error of the mean of these replicas are shown, when applicable.

Hydrogen-bonds were computed with VMD [88] with default geometrical parameters, and considering the Fluorine atoms of BF4 as possible H-bond acceptors. Dispersive (Lennard-Jones) and Coulomb energies were computed with the gmx energy module of Gromacs.

3. Results and discussion

3.1. Correlations of excess accumulation and depletion of counterions

The high degree of correlation of the distribution of cations and anions of IL in a solution is a consequence of their charges and the fact that large regions of the solution cannot be non-neutral. This implies that the accumulation of one of the ions in the vicinity of the solute requires some counterion compensation at relatively short distances. In aqueous solutions of ILs the compensations need to occur by the emergence of correlated distributions for the cations and the anions. Therefore, first we will show the emergence of these correlations despite the very different interactions the ions of a IL form with the protein. These correlations imply that the Kirkwood-Buff integrals of cations and anions assume nearly identical values in practice.

Fig. 1A shows the minimum-distance distribution functions of the cation EMIM and the anion DCA relative to Ubiquitin in the ~2 mol L^{-1} IL solution. The cation EMIM is highly concentrated on the protein surface. The density of EMIM is as much as ~7 times greater at a distance of 2.3 Å from the protein than in the reference state. The distance is typical of non-polar or dipolar interactions lacking specificity. This is confirmed by the fact that direct EMIM-protein Lennard-Jones interactions (−601 kcal mol^{-1} - Supp. Table S2) are much stronger than electrostatic interactions (−134 kcal mol^{-1}). There is a second diffuse peak at about 5 Å characteristic of a secondary solvation shell, in which the interactions with the protein might be mediated by water, the counterion, or by EMIM itself. At about 8 to 10 Å, the MDDF converges to 1.

The distribution of the anions in the same solution is different than that of the cations as a result of their hydrogen-bonding capacity. DCA is also highly concentrated at the protein surface, and the MDDF peaks at 1.9 Å and at 2.7 Å with a ~ 4 fold density augmentation relative to the reference distribution. The peak at 1.9 Å is characteristic of hydrogen-bonding, while non-specific interactions with the protein can lead to DCA accumulation at ~2.7 Å. At this concentration, DCA forms ~12 hydrogen-bonds and displays strong dispersive and electrostatic interactions with the protein (−474 and − 657 kcal mol^{-1},

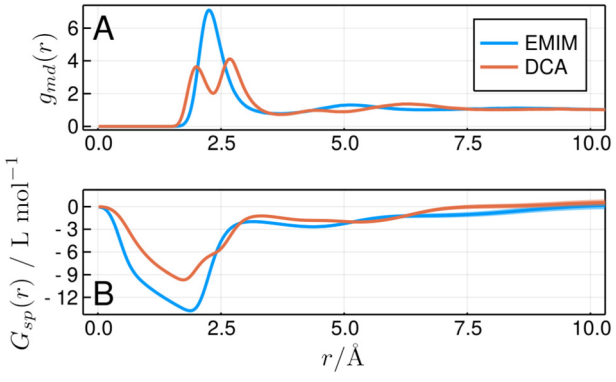

Fig. 1. A) Minimum-distance distribution functions ($g_{md}(r)$) and B) Kirkwood-Buff integrals ($G_{sp}(r)$) of the cation EMIM and the anion DCA relative to Ubiquitin in a ~ 2.0 mol L^{-1} solution of EMIMDCA in water. This figure illustrates how markedly different distribution functions can give rise to identical KB integrals, implying that the distribution functions are correlated at large distances. Similar plots for other ILs and concentrations are shown in Supp. Figs. S1-S4. Standard errors computed from 20 independent runs are shown as shaded regions (and are small and barely visible in these figures).

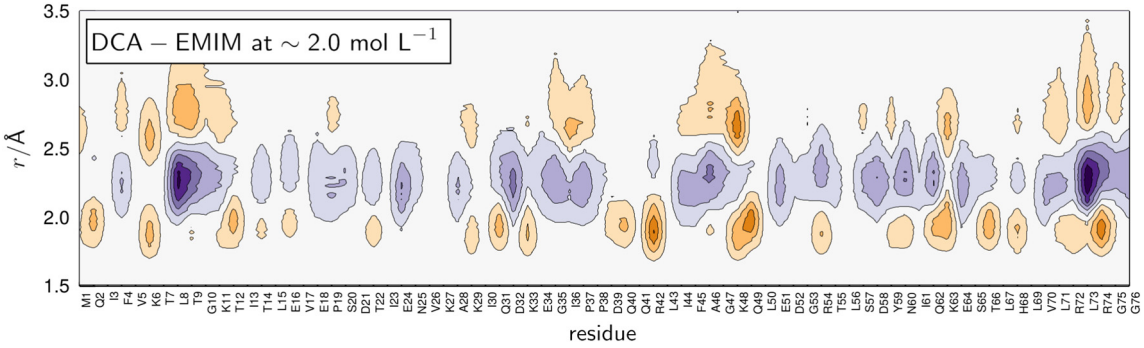

Fig. 2. Difference in densities of the ions in the vicinity of each of the protein residues at ~2.0 mol L^{-1}. The density of DCA is greater in orange regions, and the density of EMIM is greater in purple regions. The accumulation of DCA in the 2.5–3.0 Å range occurs complementarily to the accumulation of EMIM within 2.0–2.5 Å, indicating that the second peak of the DCA distribution in Fig. 1A is an anion solvation-shell mediated by the cation. Qualitatively similar plots for all other concentrations and compositions are shown in Supp. Figs. S5–S8.

respectively - Supp. Table S3). Some diffuse dips and peaks can be observed within 3 and 8 Å, and above that distance on the distribution of DCA molecules appear to be essentially uncorrelated with the protein. Thus, the MDDFs of EMIM and DCA reflect direct protein-ion interaction leading to local density augmentations at short distances. However, the nature of the interactions are different, with DCA displaying specific hydrogen-bonding and multiple well-defined solvation shells, while EMIM forms only non-specific bonds with the protein surface. Similar profiles are observed at other concentrations as shown in Supp. Figs. S1-S4.

The notable difference between the distribution functions of EMIM and DCA in Fig. 1A might suggest that, overall, one of the ions was preferentially bound to the protein relative to the other. However, as discussed above, in a solution with no other ions, this cannot be the case. Fig. 1B displays the KB integrals of EMIM and DCA computed from the minimum-distance count and using Eq. 3. At very short distances, i.e. $r < 1.5$ Å, the KB integrals obtained from MDDFs are associated to the excluded protein and solvent volumes, that is, they assume negative values because the density of the ions at those distances is zero and, thus, there is the effective exclusion of the solvent molecules from the domain. The drop of the KBI for EMIM is greater than that for DCA because the cation is a bulkier molecule. From ~1.5 Å to ~8 Å the KB integrals integrate the number of solvent molecules which are effectively correlated with the protein surface (as indicated by the MDDFs in Fig. 1A). For each ion, the integral varies according to the MDDF, with EMIM displaying one sharp increase around 2.7 Å and DCA displaying two accumulation steps associated with the peaks of its MDDF. At larger distances, the diffuse indirect correlations with the protein surface lead to the final overall excess accumulation of the ions in the protein domain, which in this illustrative example converges at 10 Å (convergence for most KBIs was obtained at 20 Å as shown in Supp. Figs. S1-S4). For these ions, the final KB integrals (at large distances) is close to zero. This means that the density augmentation of the ions in the protein domain is enough to compensate for the excluded protein volume. The water KB integral in this system is negative, as shown in Table 1 and in Supp. Fig. S1, indicating that the ions are binding the protein preferentially relative to water. Noteworthy is the fact that the KB integrals of both ions assume the same final values from about 10 Å on. This implies that the excess number is the same for the cation and the anion in the protein domain. This is a fundamental result which, as discussed, stems from the fact that the electrostatic forces will at some point lead to the correlated accumulation or depletion of the ions such that the bulk solution remains electrically neutral. Still, understanding the molecular details of how these correlations emerge on top of strikingly different protein-ion interactions and distribution functions is of fundamental importance for understanding the interactions of IL with complex solutes.

In Fig. 2 we show that the accumulation of the cation and of the anion on the surface of the protein display structural correlations. The figure displays the difference in the contribution of each residue to the minimum distance density of each ion, DCA, or EMIM, at each distance. Orange regions indicate that the density of DCA is greater than that of EMIM, and purple regions that the density of EMIM is greater than that of DCA. The first peak in the DCA minimum-distance distribution can be, now, associated with specific residues of the protein, most notably the positively charged K6, K11, K33, R42, K48, K63, and R64. Relevant contributions of some Glutamine (Q) residues can also be identified. Hydrophobic and negatively charged regions are responsible for the most important density augmentations of EMIM, particularly in the protein segments T7-L8-G9-T10, V17-E18-P19-S20, E34-G35-I36-P37, L343-I44-F45-A46, and L56-S57-D58.

We highlight the fact that the second peak of the DCA distribution is explained by its accumulation in regions following the cation. In particular, important DCA densities are found within 2.5 Å and 3.5 Å after the EMIM accumulation around T7-L8-G9-T10, E34-G35-I36-P37, and L343-I44-F45-A46. Additionally, at the N-terminal region comprising L71-R72-L73-R74-G75, containing alternating hydrophobic and positively-charged residues, a complete set of alternating interactions is formed: DCA accumulates at hydrogen-bonding distances, followed by EMIM at 2.0–2.5 Å, and finally again by DCA at 2.5–3.0 Å. Thus, density correlations between the cations and the anions can be effectively found in the solvation structures.

The same phenomenon is observed for ILs formed by other pairs of ions, independently of the nature of the chemical interactions of the ions with the protein. As shown in Fig. 3A, the MDDF of BMIM is qualitatively similar to that of EMIM in the presence of DCA, displaying a single dominant peak at 2.3 Å. BF4, on the other side, does not display a strong hydrogen-bonding character and only a small peak can be observed at ~1.9 Å (Fig. 3A), such that its distribution around the protein is qualitatively different from that of DCA. This is expected, as Fluorine

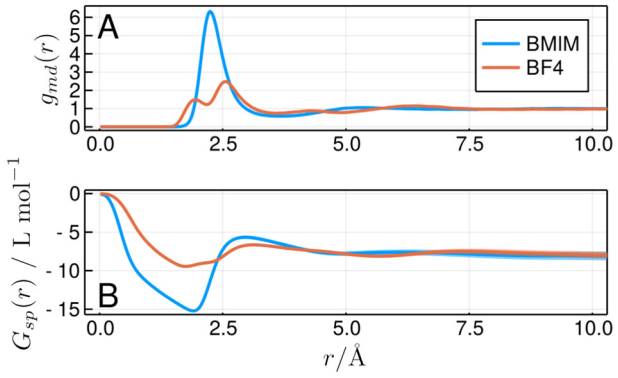

Fig. 3. A) Minimum-distance distribution functions and B) Kirkwood-Buff integrals of the cation BMIM and the anion BF4 relative to Ubiquitin in a ~2.0 mol L^{-1} solution of BMIMBF4 in water.

atoms are not good hydrogen-bonds acceptors. Effectively, BF4 forms roughly half to the number of H-bonds than DCA at this concentration, if the same geometrical parameters are considered (Supp. Table S3). Similarly, both the dispersive and electrostatic interactions of BF4 with the protein are much weaker than those of DCA (−159 and −313 kcal mol^{-1}, respectively - Supp. Table S3). The KB integrals of the ions in this system are shown in Fig. 3B, and converge in this case to the same negative value. In this case, the density augmentation of the ions in the protein domain is not enough to compensate for the excluded protein volume, and the KB integral for water is less negative than that of the ions (Table 1 and Supp. Fig. S4). Thus, the protein is preferentially hydrated in this system.

In summary, we show that the interactions of a protein with the components of an IL in water give rise to specific density profiles. However, independently of the variable chemical nature of the two ions involved, the overall excess accumulation or exclusion of the ions from the protein domain is the same, as expected to guarantee the electroneutrality of the solution at long distances from the protein. This phenomenon implies a high correlation of the distributions of the cation and of the anion, and that it is not possible to design nor predict IL-solute interactions from the chemical nature of each of the ions alone.

3.2. Effect of anion affinity to the protein on the cation distribution

The distributions of the cation and of the anion around the protein are, as shown above, correlated. Therefore, exchanging one of the ions must imply a different distribution for the corresponding counterion. First, we study the effect of exchanging DCA, a highly polar and hydrogen-bonding anion, with BF4, which is less polar and is less prone to establish hydrogen-bonds.

In Fig. 4 we compare the distribution functions and KB integrals of the anions DCA and BF4 in the presence of the same cation, EMIM. Particularly at low IL concentrations, the density augmentation of DCA at the vicinity of the protein surface is much larger than that of BF4. For example, in the ~0.5 mol L^{-1} solutions, at 1.9 Å, DCA is found in a concentration 10 times greater than that of the reference solution, while the density of BF4 at that distance is only ~2.4 greater. At ~2.3–2.5 Å the second peak of the distributions also indicate greater binding of DCA to the protein surface through non-specific interactions.

These differences in the distribution functions are reflected in the overall accumulation of the anions at the protein domain, as shown by the KB integrals in Fig. 4C and D. Notably, DCA displays positive KB integrals at the lower IL concentrations, while BF4 displays negative KB integrals at all concentrations. These results imply that DCA has a much higher affinity to the protein surface than BF4. Compared to BF4, DCA forms more hydrogen-bonds, and displays stronger dispersive and electrostatic interactions with the protein, at all concentrations (Supp. Table S3). Therefore, its strong preferential binding can be associated with favorable direct interactions with the protein surface. Similar results are obtained for DCA and BF4 in the presence of the cation BMIM (Supp. Fig. S2). In what follows, we will show how the variable properties of these anions affect the interactions of the cations with the protein surface.

The greater affinity of the anion DCA relative to BF4 has implications on the distribution of the cations of the solution, as discussed. In Fig. 5 we show how the cation EMIM is distributed in the solution, relative to the protein, in the presence of the two different anions. Fig. 5A and B show, first, that EMIM displays a greater density augmentation at the protein surface in the presence of DCA than in the presence of BF4. This effect is greater at lower IL concentrations, where the differences in affinity of the two anions to the surface are greater. While the extent

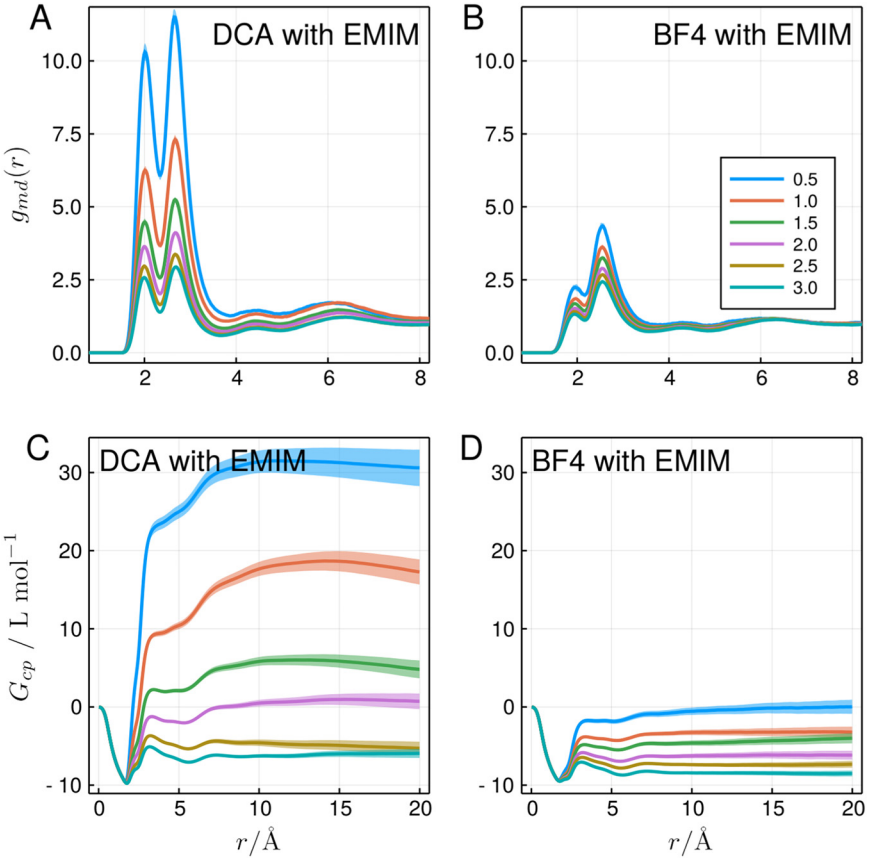

Fig. 4. DCA is a stronger binder to the protein than BF4 in the presence of the same cation, particularly at lower concentrations. Minimum-distance distribution functions, relative to the protein, of A) DCA and B) BF4, in the presence of EMIM, show that the density augmentation of DCA at the protein surface is much greater than that of BF4. This accumulation implies more positive KB integrals as shown in C) for DCA than in D) for BF4. The legend displays the reference concentrations of each simulation. Effective bulk concentrations and shown in Table 1.

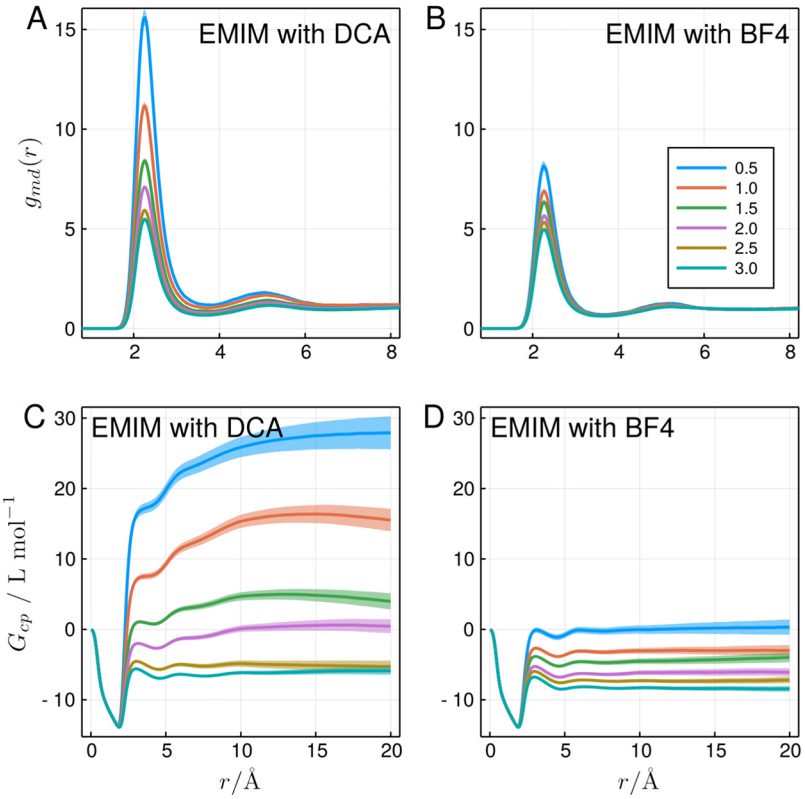

Fig. 5. EMIM is a stronger binder to the protein in the presence of DCA. Minimum-distance distribution functions of EMIM, relative to the protein, in the presence of A) DCA and B) BF4. KB integrals of EMIM in the presence of A) DCA and B) BF4.

to which the cation accumulates on the protein surface with different anions is different, it is not possible to discern any qualitative difference between the distribution curves. That is, the density augmentation of EMIM at the protein surface induced by DCA occurs by strengthening the same type of interaction EMIM displays with the protein in the presence of BF4. Finally, as expected, the KB integrals of EMIM in the presence of DCA are more positive than those of EMIM in the presence of BF4, as shown in Fig. 5C and D (and assume the same values of those of the corresponding anions, which are shown in Fig. 4C and D). Similar results are observed by exchanging the anion in ILs composed by BMIM, as shown in Supp. Figs. S9 and S10.

Therefore, the cation EMIM displays very different distributions and overall accumulations at the protein domain depending on the chemical nature of the accompanying anion. The effect is not diffuse and long-ranged, in the sense that electrostatic compensations occur by strengthening the same type of protein-cation interactions that are present at different concentrations and in the presence of different anions. EMIM-protein interaction energies (Supp. Table S2), indicate that the greater affinity of EMIM in the presence of DCA stems mainly from dispersive interactions with the protein. For example, at ~0,5 mol L^{-1}, the dispersive interactions of EMIM with the protein are −313 kcal mol^{-1} in the presence of DCA, and only −178 kcal mol^{-1} in the presence of BF4. Electrostatic interactions are, respectively, −73 and −54kcal mol^{-1}. Thus, the effect of exchanging the anion is greater on the cation dispersive interactions with the protein. At ~3.0 mol L^{-1} the surface of the protein appears to become saturated, and EMIM displays similar distribution functions and interaction energies in the presence of either of the anions.

In Fig. 6 we show the effect of exchanging the anion on the density profiles of each of the components around each protein residue. DCA accumulates more than BF4 at the protein surface, as shown by the orange regions in Fig. 6A. This density augmentation occurs particularly in the vicinity of positively charged residues, most notably K11, R42, K63, R72, and R74. Interestingly, as shown in Fig. 6B, the cation EMIM also gets further accumulated by in the presence of DCA around the same residues. Thus, despite having a positive charge, the cation is driven by the anion to the vicinity of positively charged regions on the surface of the protein to promote local charge compensation. This is consistent with cation-protein interactions being indirect and associated with stronger dispersive energies. Finally, in Fig. 6C, we show that water is excluded from the protein solvation shell by exchanging BF4 by DCA, as a consequence of the greater accumulation of DCA and EMIM molecules in this system relative to the EMIMBF4 solution.

3.3. Hydrophobicity of the cation

The exchange of the cation must also affect the distribution of the anions. Most IL cations, however, are significantly hydrophobic, such that their interactions with the protein are less specific. Here, we explore the effect of increasing the aliphatic chain of the cation into its affinity to the protein surface and correlated effects on the anion distributions.

In Fig. 7 we show the distribution functions and KB integrals of cations EMIM and BMIM in ILs formed by the DCA anion. BMIM displays a greater accumulation in the protein domain than EMIM. This is noticeable particularly at the lower concentrations of the ILs. For example, at ~0.5 mol L^{-1}, the minimum-distance distribution of EMIM at ~2.6 Å indicates a ~ 15-fold density augmentation, while BMIM displays a ~25-fold density augmentation at the same distance. These peaks are associated with non-specific interactions, particularly with non-charged residues (See latter discussion and Supp. Fig. S15). At this concentration, the dispersive interactions of BMIM with the protein are of −501 kcal mol^{-1}, while those of EMIM are of −313 kcal mol^{-1} (Supp. Table S2). Electrostatic interactions differ only slightly (−87 and −73 kcal mol^{-1}), supporting the interpretation that the interactions of the cations with the protein surface are predominantly of hydrophobic nature.

The greater density of BMIM at short distances implies greater overall accumulation of this cation at the protein domain, as indicated by the

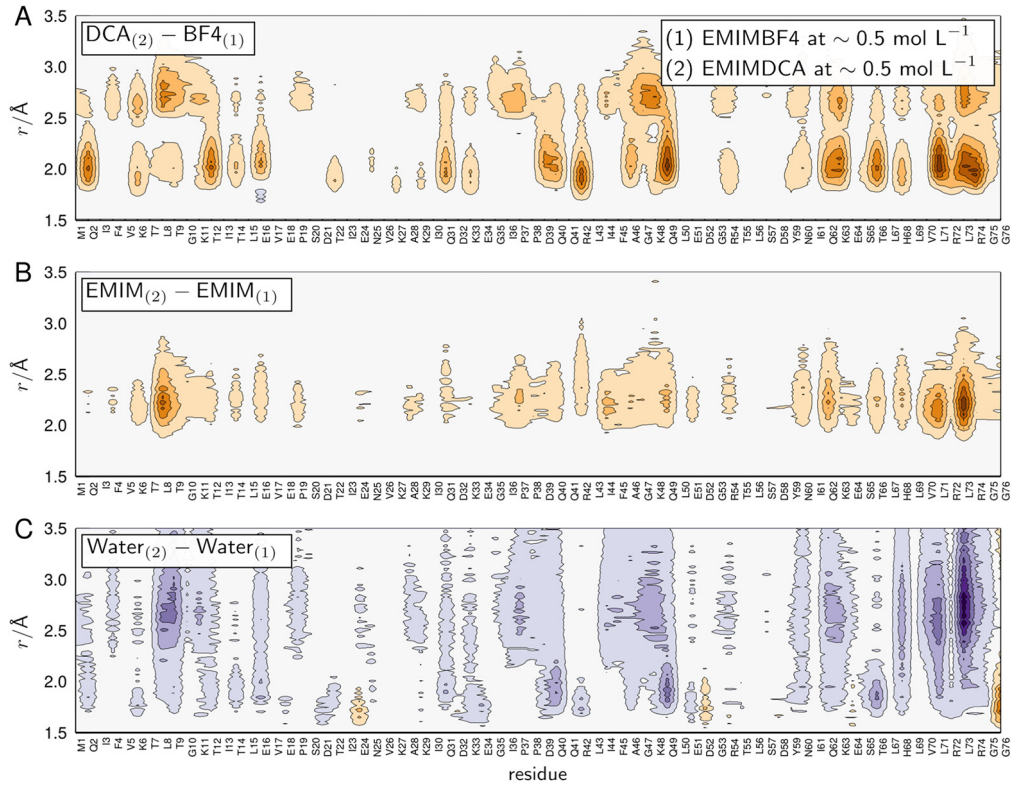

Fig. 6. Effect of anion exchange on the density of the solvent components at the vicinity of each protein residue. Orange indicates that the density in solution 2 (with DCA) is greater than in solution 1 (with BF4), and purple that density in solution 2 is greater than in solution 1. A) DCA is accumulated more than BF4, with notable density increases nearby positively charged residues. B) EMIM, in the presence of DCA, is further concentrated on the protein surface, in the same regions where DCA binds preferentially relative to BF4. C) Water is excluded from the protein surface in the EMIMDCA solution relative to the solution with EMIMBF4.

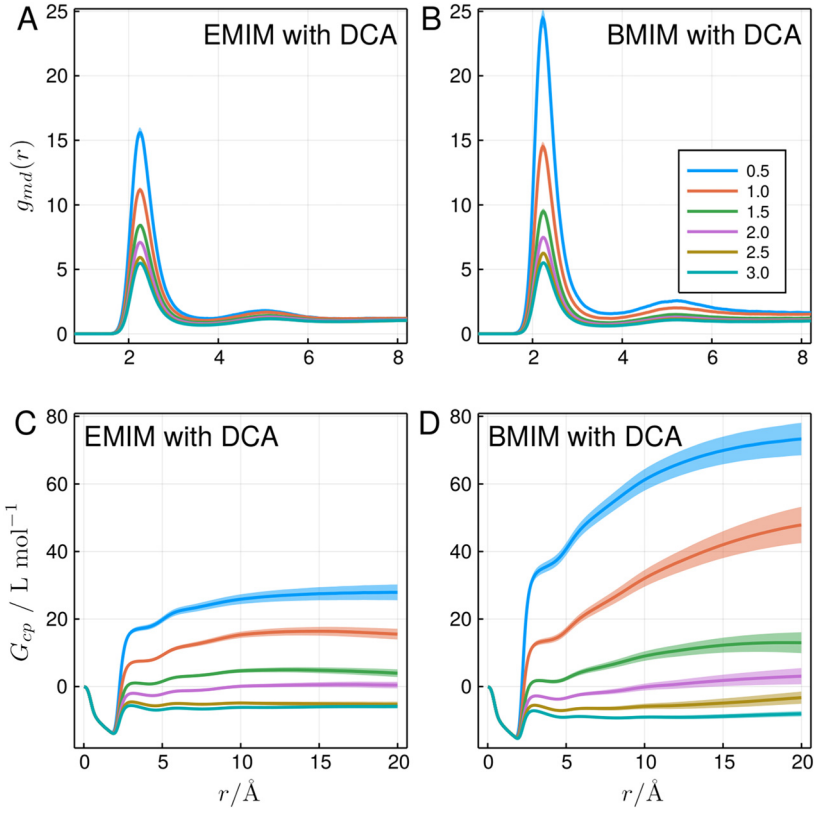

Fig. 7. Effect of augmenting the aliphatic chain of the cations on their affinity to the protein surface. Minimum-distance distribution functions of A) EMIM and B) BMIM, in the presence of DCA, are shown. Both are highly accumulated on the protein surface, particularly at low concentrations, and the increase in the aliphatic chain of the cation induces an even greater density augmentation at the protein surface. KB integrals for A) EMIM and B) BMIM in the same solutions. BMIM KB integrals are generally greater, indicating further accumulation of the cation in the protein domain. Distribution functions and KB integrals for EMIM and BMIM in the presence of BF4 are shown in Supp. Fig. S11.

KB integrals in Fig. 7C and D. For both EMIM and BMIM the KB integrals are positive at low concentrations, reflecting the preference of these ions to the protein surface relative to the bulk aqueous solutions.

Therefore BMIM, in the presence of DCA and particularly at low concentrations, has a greater affinity to the protein surface than EMIM. This must imply different affinities of the protein to the anions in the same solutions. In Fig. 8 we show the distribution functions and KB integrals of the anion DCA resulting from the exchange of the cations. Fig. 8A and B show the distribution functions of DCA relative to Ubiquitin in solutions formed by ILs with EMIM and BMIM. DCA displays important density augmentations at distances associated with hydrogen-bonding and non-specific interactions, as discussed. Both peaks at ~1.9 Å and ~2.3 Å increase, particularly at low concentrations, when the cation EMIM is replaced by BMIM. Therefore, the increase in the hydrophobicity of the cation strengthens both the hydrogen-bonding and non-specific interactions of DCA with the protein surface. The analysis of interaction energies between DCA and the protein provides an interesting view of these effects. At ~0.5 mol L^{-1}, the number of hydrogen bonds of DCA with the protein increases, but only slightly, from 8.4 to 9.3 upon cation exchange (Supp. Table S3). Dispersive interactions remain essentially unchanged (at −337 kcal mol^{-1}), but electrostatic interactions become significantly more favorable with BMIM (from −298 with EMIM to −440 kcal mol^{-1} with BMIM). Thus, increasing the cation hydrophobicity increases the nonspecific electrostatic interactions of the anions with the protein surface.

As expected, the presence of the most hydrophobic cation implies greater anion accumulation in the protein domain. This is quantified by the KB integrals shown in Fig. 8C and D, which are similar to those of the corresponding cations in the same solutions (Fig. 7C and D). Thus, DCA becomes a better binder to the protein by increasing the hydrophobic character of the associated cation in the IL preparation. This increased affinity is observed even at hydrogen-bonding distances, where the interaction of the anion with the protein surface is direct.

The correlation between the cation and the ion become more complex if analyzed in light of concentration effects. In Figs. 7 and 8 it is clear that the differences in affinities of the ions to the protein in the presence of different counterions decrease with increasing concentration of the ILs. For instance, at ~3 mol L^{-1} the KB integrals of the ions are very similar (green lines), independently of the counterion present. These concentration effects are magnified when the anion is BF4 and the overall accumulation of the ions in the protein domain is smaller.

Fig. 9 displays the variation in the local density of the solution components when the cation is exchanged. In Fig. 9A we show that, most commonly, the increased hydrophobicity of the cation leads to an increase in the density of the anion (DCA in this case) near the protein. This increased DCA density occurs both at the first solvation layer (at hydrogen-bonding distances) and at a second DCA layer (at ~2.5–3.5 Å), most notably around residues L8, F45, and L73. These three last spots are associated with the greater density of BMIM relative to EMIM, shown in Fig. 9B. BMIM displays always a greater accumulation than EMIM, particularly in hydrophobic regions of the protein surface. This greater BMIM density leads to the formation of the second DCA layer through local electrostatic compensation. As shown in Fig. 9C, water is significantly more excluded from the protein solvation shell by BMIM than by EMIM.

In Fig. 10 we show the distribution functions and KB integrals of BF4 in the presence of EMIM or BMIM. As observed for DCA, the greater affinity of BMIM to the protein promotes increased binding of BF4 to the

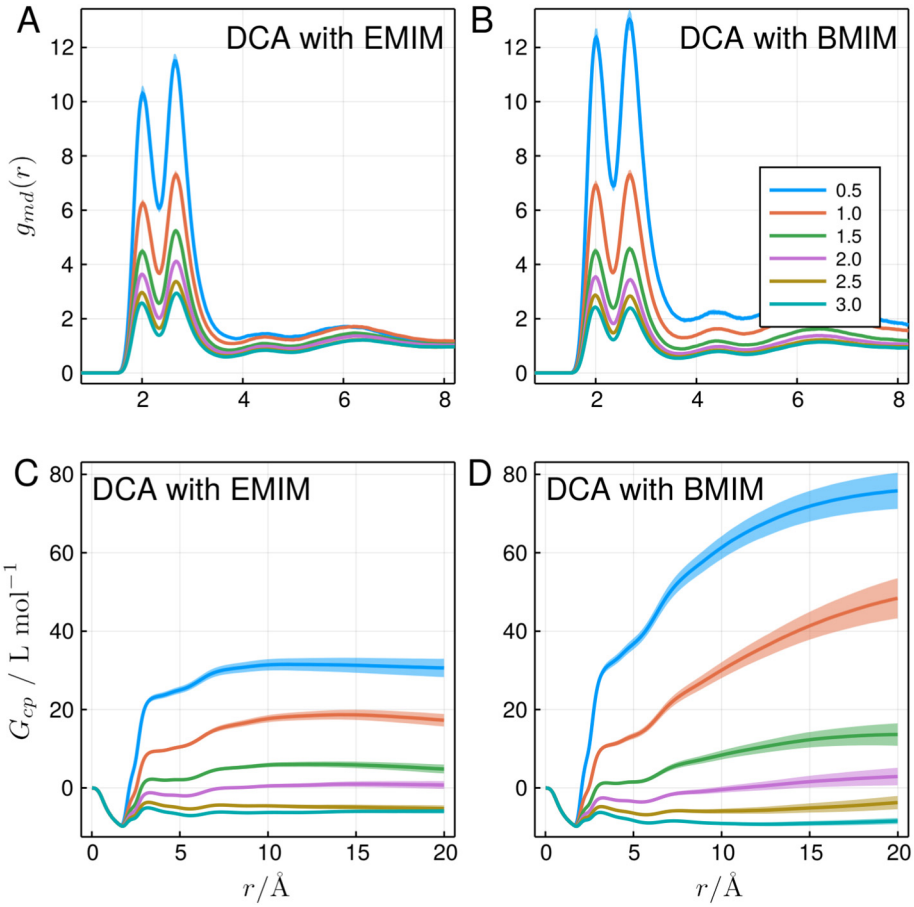

Fig. 8. DCA displays higher affinity to the protein surface in the presence of BMIM than of EMIM. Minimum-distance distribution functions of DCA in the presence A) EMIM and B) BMIM are shown. The KB integrals of DCA in the presence of A) EMIM and B) BMIM indicate greater accumulation of DCA in the protein domain in the presence of BMIM. As expected, these KB integrals are similar to those of the corresponding cations in the same solutions (Fig. 5C and D).

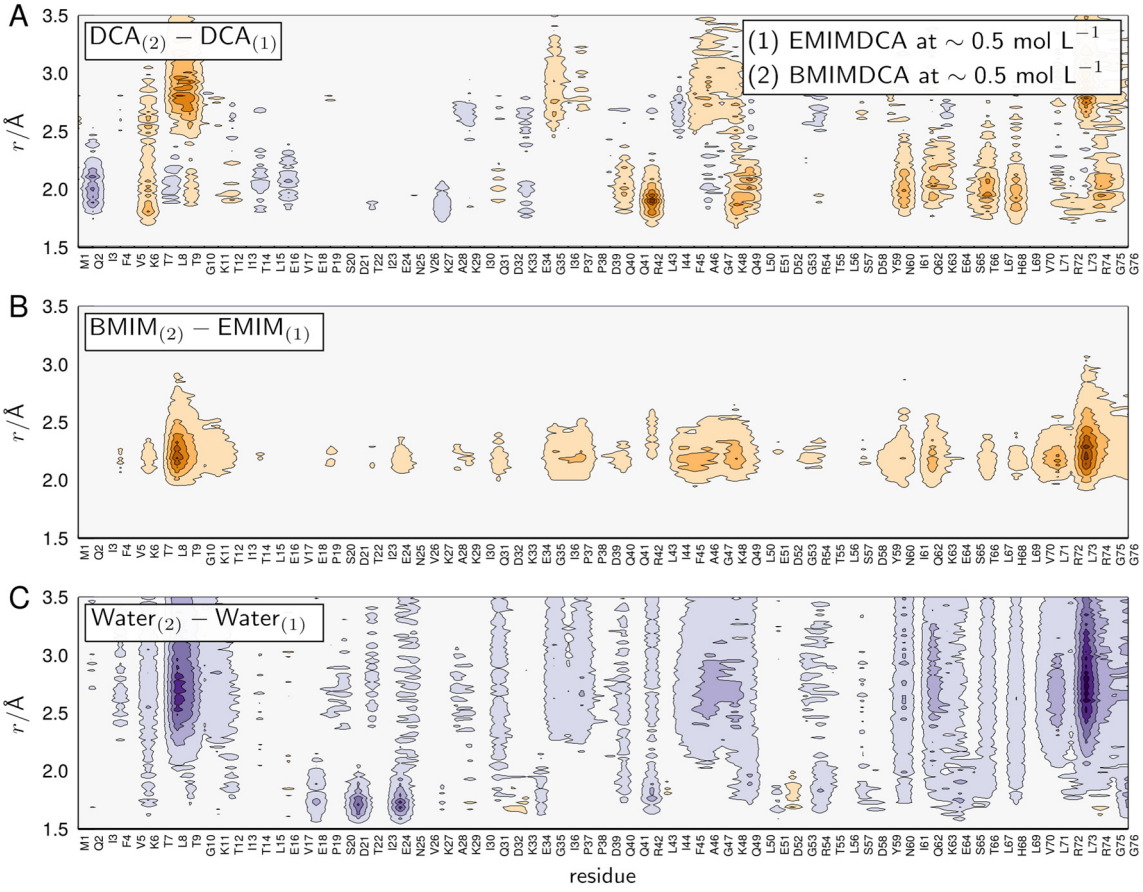

Fig. 9. Effect of cation exchange (EMIM to BMIM) on the distribution of the species at the vicinity of the protein, for ~0.5 mol L^{-1} solutions of ILs containing DCA. Increasing the hydrophobicity of the cation promotes an increased accumulation of the ions in the protein surface. Orange indicates that the density of solution 2 (with BMIM) is greater than that of solution 1 (with EMIM), and purple that the density of solution 1 is greater than that of solution 2. A) DCA density increases with the increased cation hydrophobicity, with important contributions in the second solvation layer at residues T7 to T9, F45 to K48, and R72 to G75. B) The regions of increased cation density precede the second anion layer observed in panel A. C) Water is excluded from the protein surface when the hydrophobicity of the cation is increased.

protein at low concentrations, implying higher MDDF peaks and greater KB integrals. However, concentration effects are enough to reverse this trend. At the higher concentrations, BF4 becomes less affine to the protein in the presence of BMIM than in the presence of EMIM. This can be understood by the association equilibrium of BMIM to the protein: at low concentrations the cations preferentially bind to the more hydrophobic portions of the protein surface, resulting in significant density increases near the protein surface. However, as the more hydrophobic sites of the protein surface become occupied and the concentration of the IL increases, BMIM is displaced to the solution. The preferential binding of BMIM to the protein decreases, dragging the anion altogether to the bulk solution. This picture is supported by the fact that BF4 forms fewer hydrogen bonds and displays weaker interaction energies with the protein at ~3.0 mol L^{-1} with BMIM than with EMIM (Supp. Table S3), indicating that it is effectively displaced from the protein surface. Since BF4 does not form strong specific bonds to the protein surface, the hydrophobic interactions between cation molecules dominate the distribution of the components in the solution. This is different from DCA, which by forming strong specific bonds to the protein surface, promotes dehydration at a wider concentration range, independently of the saturation of the hydrophobic sites of the protein surface by the cation. Thus, a cation with greater aliphatic chain might lead to either decreased or increased affinities of the counterion to the protein, depending on the IL concentration. Lower concentrations imply greater preferential binding of hydrophobic groups to the protein, but at higher concentrations, the amphiphilic character of the cations might lead to a decreased accumulation of both ions in the protein domain when the more hydrophobic portions of the protein surface are saturated.

3.4. Preferential binding coefficients

The above analyses can be summarized in terms of preferential binding coefficients of the IL, (cosolvent *c*, identical for the cation and the anion), to the protein, *p*: Γ_{cp}. A positive preferential binding coefficient for a cosolvent suggests that the solute surface is stabilized by the presence of the cosolvent. Qualitatively, $\Gamma_{cp} > 0$ implies that the cosolvent interacts favorably with the protein surface relative to water, thus adding the cosolvent favors structures with greater surface area. Usually, this is interpreted as suggesting a denaturing role for the cosolvent, although the thermodynamic effect on the protein structure depends on the interactions of the solvent components with the denatured protein states. In other words, if Γ_{cp} is positive, the chemical potential of the protein surface is decreased by the addition of the cosolvent (the IL): the protein is preferentially solvated by the IL. If, on the contrary, Γ_{cp} is negative, the IL is excluded from the protein domain, meaning that the chemical potential of the protein surface increases by the addition of the cosolvent. In this case, the protein is preferentially hydrated (the preferential hydration coefficient Γ_{wp} is positive).

Fig. 11 illustrates the preferential binding coefficients of the ILs to Ubiquitin in the lowest and the highest concentrations studied here, with the four IL compositions. As shown in Fig. 11A, $\Gamma_{cp}$is positive for EMIMDCA and BMIMDCA at 0.5 mol L^{-1}. This implies that the chemical potential of the protein surface is decreased by the addition of the ILs at this concentration. The concentration effects can be sorted out by observing Fig. 11B: While Γ_{cp} for the ILs at 3 mol L^{-1} is still positive for EMIMDCA, it is negative for BMIMDCA, implying that in this last case the protein is preferentially hydrated. In other words, the chemical

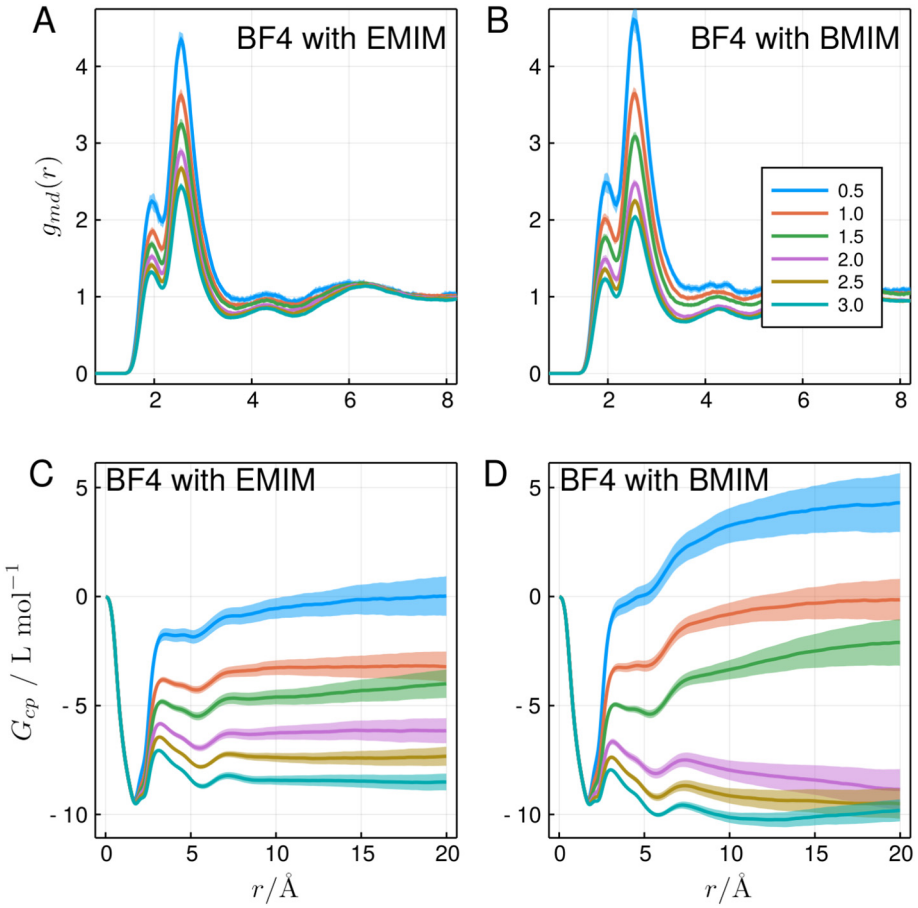

Fig. 10. The effect of cation hydrophobicity in the preferential binding of BF4 to the protein surface is concentration-dependent. Distribution functions of BF4 in the presence of A) EMIM and B) BMIM show greater differences at low concentrations. The KB integrals of BF4 in the presence of A) EMIM and B) BMIM show that the anion has greater affinity to the protein surface with BMIM at low concentrations (blue), but with EMIM at higher concentrations (green).

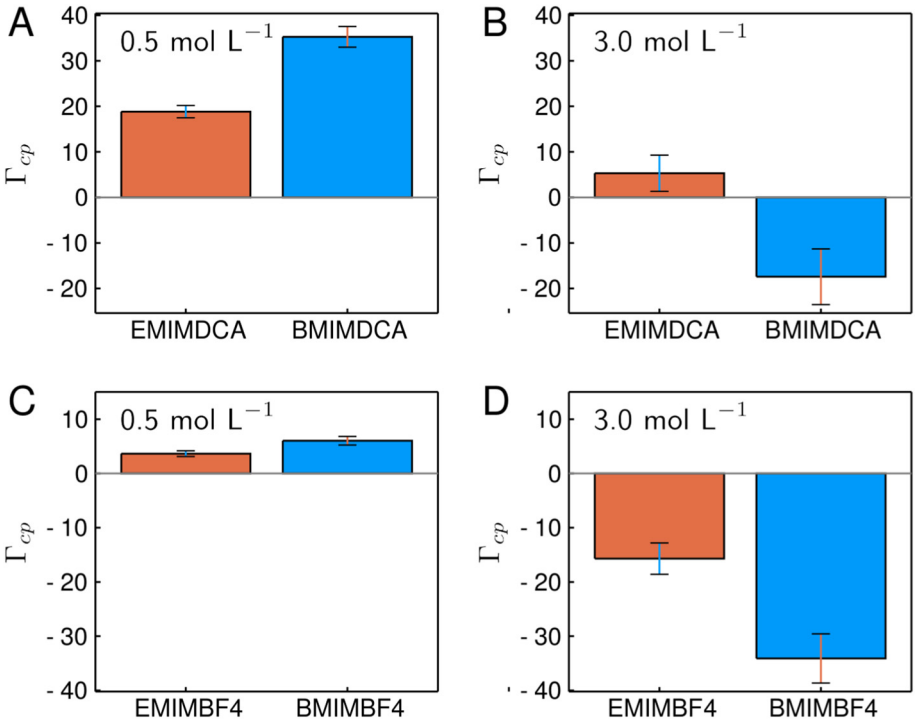

Fig. 11. Preferential interaction parameters, Γ_{cp}, of the ILs with the protein, with different compositions and concentrations. A) EMIMDCA and BMIMDCA at ~0.5 mol L^{-1}. B) EMIMDCA and BMIMDCA at ~3.0 mol L^{-1}. C) EMIMBF4 and BMIMBF4 at ~0.5 mol L^{-1}. D) EMIMBF4 and BMIMBF4 at ~3.0 mol L^{-1}. Preferential interaction parameters for all ILs and concentrations, and preferential hydration parameters, are shown in Supp. Fig. S13.

potential of the protein surface increases by the addition of BMIMDCA at ~3 mol L^{-1}.

The effect of anion exchange can be observed by comparing Fig. 11A and C, or B and D. DCA is a stronger binder to the protein surface than BF4, resulting in greater (more positive) preferential interaction parameters in all cases. At 0.5 mol L^{-1} Ubiquitin interactions with the ILs are always favored relative to water, and the protein is preferentially dehydrated. However, the dehydration is smaller with BF4 than with DCA. At 3.0 mol L^{-1}.

Thus, at low concentrations, the ILs tend to prefer the protein surface relative to the bulk solution. The anion plays a crucial role in this preferential binding, with DCA promoting much greater dehydration of the protein than BF4. At high concentrations, the ILs become preferentially excluded from the protein domain in all but the EMIMDCA solution.

To understand why preferential binding coefficients are positive at low concentrations and negative at high concentrations for the ILs, particularly in the presence of BMIM, we studied the protein-cation and protein-water interactions at the first protein solvation layer. Fig. 12A shows that the number of cation ions in the first solvation shell of the protein is greater for BMIM than for EMIM, as could be predicted from its greater hydrophobic character. Effectively, as shown in Fig. 12B, dispersive (Lennard-Jones) interactions are the dominant protein-cation energies. Interestingly, Fig. 12C shows that the total protein-cation interaction energy per molecule in the first solvation shell increases (becomes less favorable) with increasing concentration, indicating that the most affine and specific cation interaction sites of the protein are saturated. And, finally, Fig. 12D shows that the number of water molecules in the first solvation shell decreases with increasing IL concentration.

Figs. 12A and D, in particular, show that BMIM is associated with the protein in greater numbers at low concentrations than EMIM, explaining its greater preferential binding coefficients. However, at ~3 mol L^{-1} the number of EMIM or BMIM molecules in the first solvation shell of the protein are similar. The number of water molecules in the presence of one or other cation in the first protein solvation shell is also similar at the higher concentration. Thus, the protein experiences similar solvation shells, in terms of number of ions and water, with either cation in the solution. ILs formed by BMIM, however, display much lower preferential binding coefficients (Fig. 11) than EMIM, and this is explained by the fact that water concentration is lower in the BMIM solutions. For example, at ~3 mol L^{-1} BMIMDCA, water concentration is ~22.3 mol L^{-1}, while at the same EMIMDCA concentration, water concentration is ~27.9 mol L^{-1} (see Supp. Table S1). Thus, if the solvation shell numbers are similar, a smaller water concentration implies an effective greater preferential hydration. Additionally, one could suspect that cation self-association in the bulk solution could be reducing its binding affinity to the protein. We computed the cation-cation distribution functions in aqueous IL solutions (without the protein) to probe this possibility (Supp. Fig. S25). While the cations effectively self-associate, the concentration dependence of this self-association does not seem to justify the observed variations in protein preferential binding coefficients.

In summary, the concentration dependence of preferential binding and preferential hydration coefficients appear to be explained by a

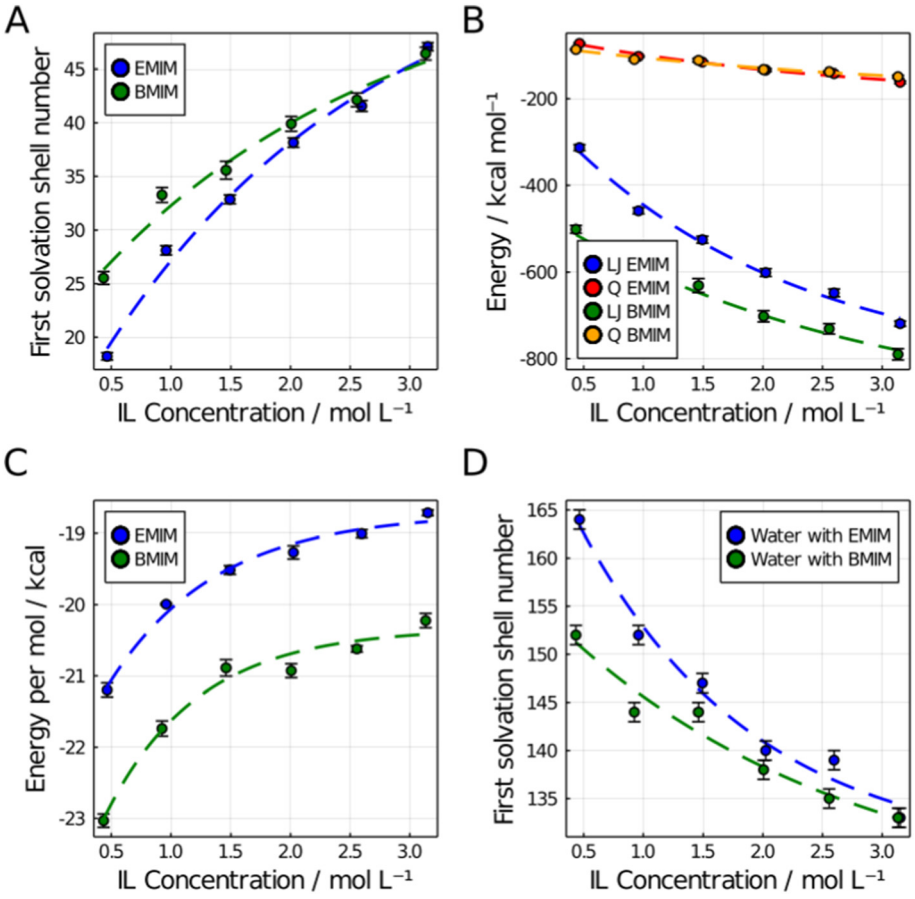

Fig. 12. Short-range interactions of the protein by IL cations in the presence of the DCA anion. A) First solvation shell number (up to 3.8 Å). B) Lennard-Jones (LJ) and electrostatic (Q) interaction energies. C) Total interaction energy per molecule in the first solvation shell. D) First solvation shell number of water (up to 2.4 Å). Dispersive forces dominate protein-cation interactions. At higher concentrations the solvation shells of the protein become similar with EMIM or BMIM. A similar figure for the ILs composed by the BF4 anion is available as Supp. Fig. S14.

progressive saturation of the solvation shell with the IL cations, accompanied by the smaller water concentration at bulk for the larger IL cation.

3.5. Counterion effects on the nature of protein-ion interactions

Minimum-distance distribution function can be decomposed into the contributions of solute or solvent groups [43]. In Figs. 13 and 14 we show the decomposition of the MDDFs of the ionic liquid relative to the protein decomposed into the contributions of the protein types of residues. In essence, the decomposition of the MDDFs shows how frequently each type of residue is the closest to any atom of the solute, at each distance. We decompose the MDDFs in the contributions of polar (Gln, Tyr, etc. - green), neutral (Ala, Phe, etc. - grey), acidic (Glu, Asp - red) and basic (Lys, Arg, His - blue) residues, following the classification and color scheme of VMD [88].

For example, in Fig. 13A, we show that the EMIM cation display a ~7.1 fold increase in local density at ~2,3 Å from the protein atoms, relative to bulk density (black), at 2 mol L^{-1}. This peak is composed of a contribution of ~2.8 density increase associated to polar residues (green), ~2.0 from neutral residues (grey), and ~ 1.2 around basic and acidic residues (red and blue). Thus, EMIM is found most frequently interacting directly with polar and neutral residues relative to charged (basic or acidic) residues, at the distance of the most important MDDF peak. Here, we want to compare these contributions to those of the residue types when the cation or the anion is exchanged.

In Fig. 13B we show the same decomposition of Fig. 13A but exchanging the anion DCA with BF4. The total peak decreases (from 7.1 to 5.7) because DCA is a greater binder to the protein surface, as discussed above. The absolute contribution of charged residues is reduced from 1.2 to 0.9 (−25%) for basic residues and from 1.1 to 1.0 for acidic residues (−9%). Polar and neutral residues contribute to a decrease in relative density of 0.5 each (2.8 to 2.3, or −18%, for polar and 2.0 to 1.5, or −25%, for neutral residues). Thus, the effect of exchanging the anion is particularly small in the vicinity of acidic residues, which form attractive electrostatic interactions with the cation. The exchange of the anion affects the weaker interactions of the cation with the protein surface, particularly the dispersive ones with neutral residues and, likely, the indirect interactions to positively charged residues which are mediated by the anion. Similar conclusions can be drawn from Fig. 13C and D, which show that anion exchange in the presence of BMIM essentially does not affect BMIM accumulation at the vicinity of acidic residues, while the total peak at 2.3 Å is reduced.

Finally, Fig. 14 shows the effect of the cation exchange in the distribution functions of the anions. The interesting feature to be noted is that the second peak of the distributions of the anions are more affected than the first peak. For instance, for DCA, the second peak is greater than the first peak with EMIM (Fig. 14A), while it is shorter than the first peak with BMIM (Fig. 14B). A similar decrease in the second peak is observed for BF4.

The first peaks, at hydrogen-bonding distances, are mostly composed by interactions with polar and basic residues, as expected. These interactions are not clearly affected by cation exchange. The second peak has important contributions of polar and basic residues, but also neutral residues. All these interactions are reduced with the increase in the hydrophobicity of the cation. Therefore, the more specific

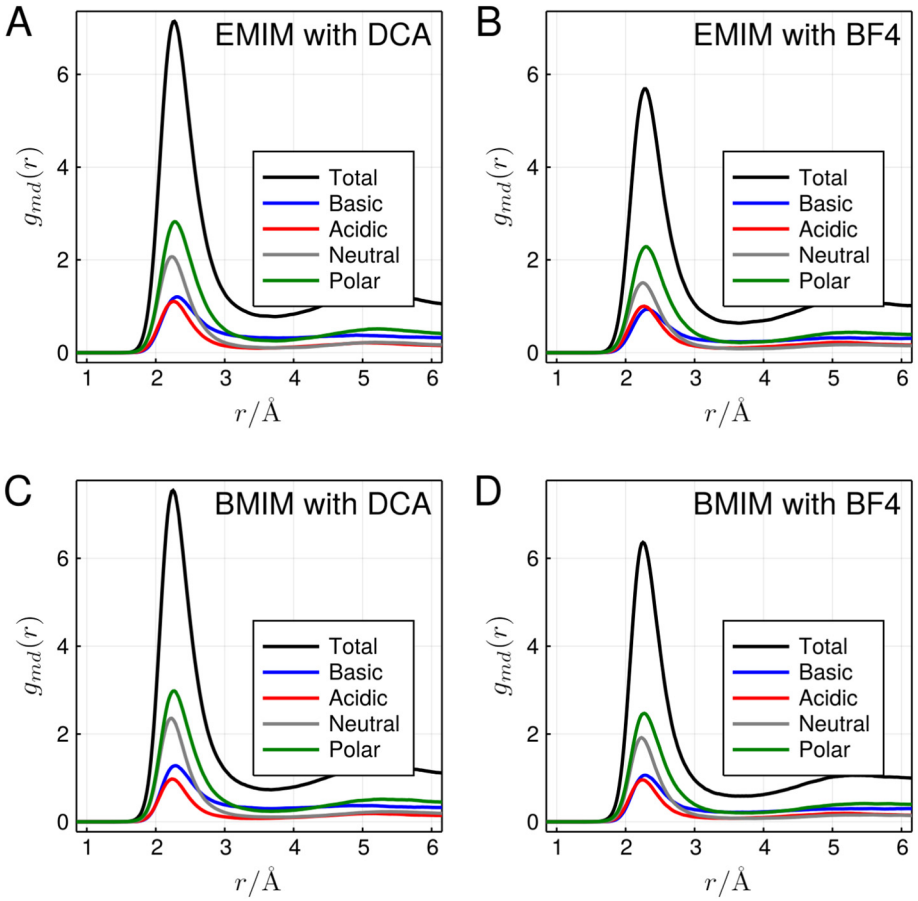

Fig. 13. Effect of anion exchange in the distribution functions of the cations: discerning the contributions of each residue type, at an IL concentration of ~2.0 mol L^{-1}. A and B) EMIM distributions in the presence of DCA or BF4. C and D) BMIM distributions in the presence of DCA or BF4. DCA promotes a much higher accumulation of the cations on the protein surface than BF4, accumulation that is particularly higher at neutral and polar residues. Supplementary Figs. S15-S18 display similar results for other IL concentrations.

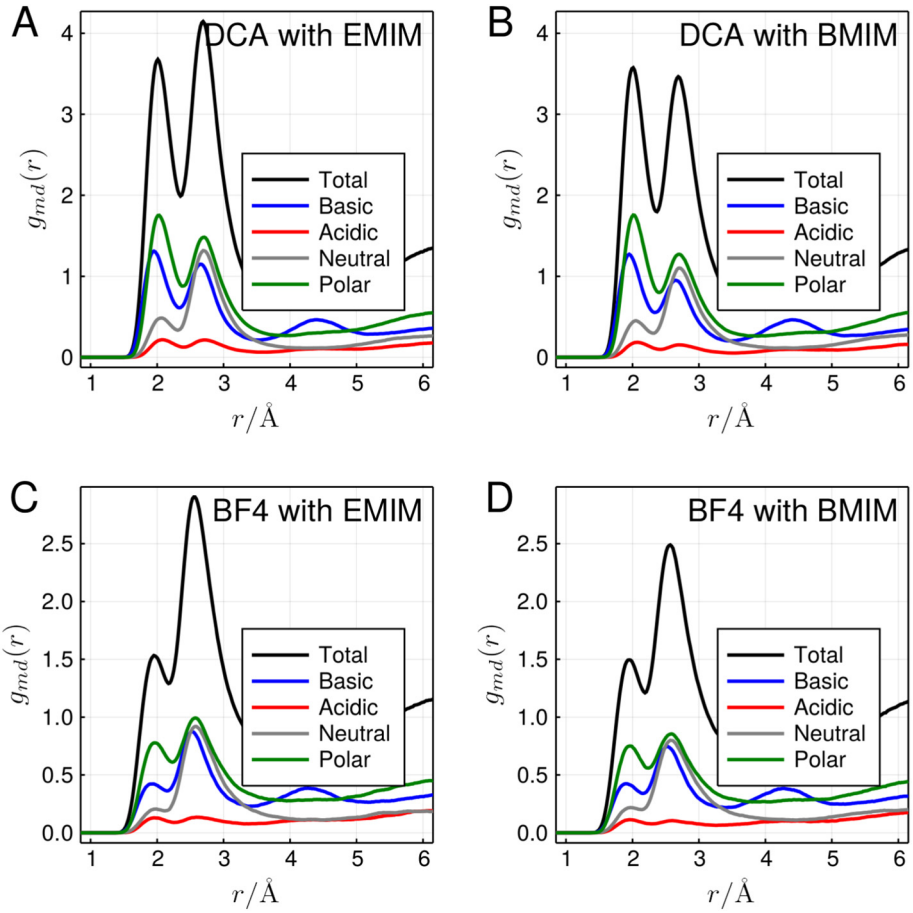

Fig. 14. Effect of cation exchange in the distribution functions of the anions: discerning the contributions of each residue type, at a IL concentration of ~2.0 mol L^{-1}. A and B) DCA distributions exchanging EMIM with BMIM. The increase in cation hydrophobicity leads to a decrease of the second peak, associated with non-specific interactions. C and D) The second peak of BF4 distributions are reduced with BMIM, an effect which is magnified at greater IL concentrations (see Supp. Figs. S19 to S24).

interactions of the anions are preserved upon cation exchange, with a reduced binding of the anions to the protein surface associated with non-specific interactions. This is similar to what was observed in cation distributions upon anion exchange, except that here the small effect on specific interactions can be directly discerned from the preservation of the hydrogen-bonding peak.

4. Conclusion

We study the molecular basis of protein interactions with ionic liquids using minimum-distance distribution functions, focusing on the effects of exchanging counterions in the distributions of the cosolvents relative to the protein. Because of the required electroneutrality of the solutions in bulk, the distributions of the cations and anions of the IL are correlated. The DCA anion, that forms strong hydrogen bonds to the protein surface, leads to a great accumulation of both the IL ions at the protein surface, but this effect can be reversed by large hydrophobic cations at the larger concentrations probed. Similarly, the extent of the accumulation of the cations in the protein domain is very much dependent on the nature of the anion. We show that the stronger and most specific interactions the ions form with the protein surface are preserved upon counterion exchange, but less specific interactions of each ion at the second and third solvation shells are modulated by the variable counterion nature and concentration. Therefore, IL composition and concentration can be varied to provide solutions with stabilizing or destabilizing roles on protein structures, and a rationale for such solvent design is provided.

CRediT authorship contribution statement

Vinicius Piccoli developed the research, ran simulations, analyzed data and wrote the manuscript.

Leandro Martínez designed research, analyzed data, obtained funding and wrote the manuscript.

Declaration of competing interest

The authors declare that they have no known competing financial interests or personal relationships that could have appeared to influence the work reported in this paper.

Acknowledgements

The authors thank the financial support of CNPq (V.P., grant 130558/2018-4), and of FAPESP (grants 2010/16947-9, 2013/08293-7, 2018/24293-0, 2018/14247-9, and 2018/24293-0). We also acknowledge the valuable insights provided by anonymous reviewers.

Appendix A. Supplementary data

Details of the molecular systems simulated, hydrogen-bonding analysis and interaction energies, and figures similar to those of the manuscript but for all concentrations studied. Supplementary data to this article can be found online at doi:https://doi.org/10.1016/j.molliq.2020.114347.

References

[1] T. Welton, Room-temperature ionic liquids. Solvents for synthesis and catalysis, Chem. Rev. 99 (1999) 2071–2084.
[2] T. Kobayashi, J.E.S.J. Reid, S. Shimizu, M. Fyta, J. Smiatek, The properties of residual water molecules in ionic liquids: a comparison between direct and inverse Kirkwood-Buff approaches, Phys. Chem. Chem. Phys. 19 (2017) 18924–18937.
[3] J. Smiatek, Aqueous ionic liquids and their effects on protein structures: an overview on recent theoretical and experimental results, J. Phys. Condens. Matter. 29 (2017), 233001.
[4] M. Armand, F. Endres, D.R. MacFarlane, H. Ohno, B. Scrosati, Ionic-liquid materials for the electrochemical challenges of the future, Nat. Mater. 8 (2009) 621–629.
[5] V.I. Pârvulescu, C. Hardacre, Catalysis in ionic liquids, Chem. Rev. 107 (2007) 2615–2665.
[6] T. Itoh, Ionic liquids as tool to improve enzymatic organic synthesis, Chem. Rev. 117 (2017) 10567–10607.
[7] J.P. Hallett, T. Welton, Room-temperature ionic liquids: solvents for synthesis and catalysis. 2, Chem. Rev. 111 (2011) 3508–3576.
[8] K. Fujita, M. Forsyth, D.R. MacFarlane, R.W. Reid, G.D. Elliott, Unexpected improvement in stability and utility of cytochrome c by solution in biocompatible ionic liquids, Biotechnol. Bioeng. 94 (2006) 1209–1213.
[9] S.Y. Lee, I. Khoiroh, C.W. Ooi, T.C. Ling, P.L. Show, Recent advances in protein extraction using ionic liquid-based aqueous two-phase systems, Separation & Purification Reviews 46 (2017) 291–304.
[10] D.F. Kennedy, C.J. Drummond, T.S. Peat, J. Newman, Evaluating protic ionic liquids as protein crystallization additives, Cryst. Growth Des. 11 (2011) 1777–1785.
[11] L. Harada, J. Pereira, W. Campos, E. Silva, C. Moutinho, M. Vila, J. Oliveira Jr, J. Teixeira, V. Balcão, M. Tubino, Insights into protein-ionic liquid interactions aiming at macromolecule delivery systems, J. Braz. Chem. Soc. (2018)https://doi.org/10.21577/0103-5053.20180141.
[12] V.W. Jaeger, J. Pfaendtner, Structure, dynamics, and activity of xylanase solvated in binary mixtures of ionic liquid and water, ACS Chem. Biol. 8 (2013) 1179–1186.
[13] V. Jaeger, P. Burney, J. Pfaendtner, Comparison of three ionic liquid-tolerant cellulases by molecular dynamics, Biophys. J. 108 (2015) 880–892.
[14] Y. Zhou, B. Pérez, W. Hao, J. Lv, R. Gao, Z. Guo, The additive mutational effects from surface charge engineering: a compromise between enzyme activity, thermostability and ionic liquid tolerance, Biochem. Eng. J. 148 (2019) 195–204.
[15] K.G. Sprenger, J. Pfaendtner, Using molecular simulation to study biocatalysis in ionic liquids, Methods Enzymol. 577 (2016) 419–441.
[16] X. Liu, Y. Nie, Y. Liu, S. Zhang, A.L. Skov, Screening of ionic liquids for keratin dissolution by means of COSMO-RS and experimental verification, ACS Sustain. Chem. Eng. 6 (2018) 17314–17322.
[17] S. Zheng, Y. Nie, S. Zhang, X. Zhang, L. Wang, Highly efficient dissolution of wool keratin by dimethylphosphate ionic liquids, ACS Sustain. Chem. Eng. 3 (2015) 2925–2932.
[18] Z. Meng, X. Zheng, K. Tang, J. Liu, Z. Ma, Q. Zhao, Dissolution and regeneration of collagen fibers using ionic liquid, Int. J. Biol. Macromol. 51 (2012) 440–448.
[19] A. Biswas, R.L. Shogren, D.G. Stevenson, J.L. Willett, P.K. Bhowmik, Ionic liquids as solvents for biopolymers: acylation of starch and zein protein, Carbohydr. Polym. 66 (2006) 546–550.
[20] J. Stanton, Y. Xue, P. Pandher, L. Malek, T. Brown, X. Hu, D. Salas-de la Cruz, Impact of ionic liquid type on the structure, morphology and properties of silk-cellulose biocomposite materials, Int. J. Biol. Macromol. 108 (2018) 333–341.
[21] D. Harries, J. Rösgen, A practical guide on how osmolytes modulate macromolecular properties, Methods Cell Biol. 84 (2008) 679–735.
[22] H.-J. Tung, J. Pfaendtner, Kinetics and mechanism of ionic-liquid induced protein unfolding: application to the model protein HP35, Molecular Systems Design & Engineering 1 (2016) 382–390.
[23] P.H. Yancey, Organic osmolytes as compatible, metabolic and counteracting cytoprotectants in high osmolarity and other stresses, J. Exp. Biol. 208 (2005) 2819–2830.
[24] D.W. Bolen, I.V. Baskakov, The osmophobic effect: natural selection of a thermodynamic force in protein folding, J. Mol. Biol. 310 (2001) 955–963.
[25] S.N. Timasheff, The control of protein stability and association by weak interactions with water: how do solvents affect these processes? Annu. Rev. Biophys. Biomol. Struct. 22 (1993) 67–97.
[26] D.W. Bolen, Protein stabilization by naturally occurring osmolytes, Methods Mol. Biol. 168 (2001) 17–36.
[27] A.M. Hyde, S.L. Zultanski, J.H. Waldman, Y.-L. Zhong, M. Shevlin, F. Peng, General Principles and Strategies for Salting-out Informed by the Hofmeister Series, 2017https://doi.org/10.1021/acs.oprd.7b00197.
[28] K. Fujita, Ionic liquids as stabilization and refolding additives and solvents for proteins, Adv. Biochem. Eng. Biotechnol. 168 (2019) 215–226.
[29] M. Klähn, G.S. Lim, P. Wu, How ion properties determine the stability of a lipase enzyme in ionic liquids: a molecular dynamics study, Phys. Chem. Chem. Phys. 13 (2011) 18647–18660.
[30] P.R. Burney, J. Pfaendtner, Structural and dynamic features of Candida rugosa lipase 1 in water, octane, toluene, and ionic liquids BMIM-PF6 and BMIM-NO3, J. Phys. Chem. B 117 (2013) 2662–2670.
[31] C. Schröder, Proteins in ionic liquids: current status of experiments and simulations, Top. Curr. Chem. 375 (2017) 25.
[32] D. Zhao, M. Wu, Y. Kou, E. Min, Ionic liquids: applications in catalysis, Catal. Today 74 (2002) 157–189.
[33] J. Wilkes, Properties of ionic liquid solvents for catalysis, J. Mol. Catal. A Chem. 214 (2004) 11–17.
[34] T.L. Greaves, C.J. Drummond, Protic ionic liquids: properties and applications, Chem. Rev. 108 (2008) 206–237.
[35] J.M. Otero-Mato, V. Lesch, H. Montes-Campos, J. Smiatek, D. Diddens, O. Cabeza, L.J. Gallego, L.M. Varela, Solvation in ionic liquid-water mixtures: a computational study, J. Mol. Liq. 292 (2019), 111273.
[36] G.S. Lim, M. Klähn, On the stability of proteins solvated in imidazolium-based ionic liquids studied with replica exchange molecular dynamics, J. Phys. Chem. B 122 (2018) 9274–9288.
[37] A. Schindl, M.L. Hagen, S. Muzammal, H.A.D. Gunasekera, A.K. Croft, Proteins in ionic liquids: reactions, applications, and futures, Front Chem 7 (2019) 347.
[38] P.R. Burney, E.M. Nordwald, K. Hickman, J.L. Kaar, J. Pfaendtner, Molecular dynamics investigation of the ionic liquid/enzyme interface: application to engineering enzyme surface charge, Proteins 83 (2015) 670–680.
[39] J. Smiatek, Theoretical and computational insight into solvent and specific ion effects for polyelectrolytes: the importance of local molecular interactions, Molecules 25 (2020)https://doi.org/10.3390/molecules25071661.
[40] J.G. Kirkwood, F.P. Buff, The statistical mechanical theory of solutions. I, J. Chem. Phys. 19 (1951) 774–777.
[41] K.E. Newman, Kirkwood–Buff solution theory: derivation and applications, Chem. Soc. Rev. 23 (1994) 31–40.
[42] V. Pierce, M. Kang, M. Aburi, S. Weerasinghe, P.E. Smith, Recent applications of Kirkwood-Buff theory to biological systems, Cell Biochem. Biophys. 50 (2008) 1–22.
[43] L. Martínez, S. Shimizu, Molecular interpretation of preferential interactions in protein solvation: a solvent-shell perspective by means of minimum-distance distribution functions, J. Chem. Theory Comput. 13 (2017) 6358–6372.
[44] I.P. de Oliveira, I.P. de Oliveira, L. Martínez, The shift in urea orientation at protein surfaces at low pH is compatible with a direct mechanism of protein denaturation, Phys. Chem. Chem. Phys. 22 (2020) 354–367.
[45] P.K. Mehrotra, D.L. Beveridge, Structural analysis of molecular solutions based on quasi-component distribution functions. Application to [H_2CO]aq at 25 °C, J. Am. Chem. Soc. 102 (1980) 4287–4294.
[46] K. Coutinho, R. Rivelino, H.C. Georg, S. Canuto, The sequential qm/mm method and its applications to solvent effects in electronic and structural properties of solutes, in: S. Canuto (Ed.), Solvation Effects on Molecules and Biomolecules, Springer 2008, pp. 159–189.
[47] V. Zeindlhofer, D. Khlan, K. Bica, C. Schröder, Computational analysis of the solvation of coffee ingredients in aqueous ionic liquid mixtures, RSC Adv. 7 (2017) 3495–3504.
[48] M. Mezei, Modified proximity criteria for the analysis of the solvation of a polyfunctional solute, Molec. Simul. 1 (1988) 327–332.
[49] S.-C. Ou, B.M. Pettitt, Solute-solvent energetics based on proximal distribution functions, J. Phys. Chem. B 120 (2016) 8230–8237.
[50] B.M. Baynes, B.L. Trout, Proteins in mixed solvents: a molecular-level perspective, J. Phys. Chem. B 107 (2003) 14058–14067.
[51] W. Song, R. Biswas, M. Maroncelli, Intermolecular interactions and local density augmentation in supercritical solvation: a survey of simulation and experimental results, J. Phys. Chem. A 104 (2000) 6924–6939.
[52] A.C. Furlan, F.W. FÁvero, J. Rodriguez, D. Laria, M.S. Skaf, Solvation in supercritical fluids, in: S. Canuto (Ed.), Solvation Effects on Molecules and Biomolecules 2008, pp. 433–453.
[53] I.P. Oliveira, L. Martínez, Molecular basis for competitive solvation of the Burkholderia cepacia lipase by sorbitol and urea, Phys. Chem. Chem. Phys. 18 (2016) 21797–21808.
[54] E.A. Oprzeska-Zingrebe, J. Smiatek, Aqueous ionic liquids in comparison with standard co-solutes: differences and common principles in their interaction with protein and DNA structures, Biophys. Rev. 10 (2018) 809–824.
[55] M.A. Schroer, J. Michalowsky, B. Fischer, J. Smiatek, G. Grübel, Stabilizing effect of TMAO on globular PNIPAM states: preferential attraction induces preferential hydration, Phys. Chem. Chem. Phys. 18 (2016) 31459–31470.
[56] I.L. Shulgin, E. Ruckenstein, A protein molecule in an aqueous mixed solvent: fluctuation theory outlook, J. Chem. Phys. 123 (2005), 054909.
[57] I.L. Shulgin, E. Ruckenstein, A protein molecule in a mixed solvent: the preferential binding parameter via the Kirkwood-Buff theory, Biophys. J. 90 (2006) 704–707.
[58] S. Weerasinghe, P.E. Smith, A Kirkwood−Buff derived force field for mixtures of urea and water, J. Phys. Chem. B 107 (2003) 3891–3898.
[59] P.E. Smith, Chemical potential derivatives and preferential interaction parameters in biological systems from Kirkwood-Buff theory, Biophys. J. 91 (2006) 849–856.
[60] S. Shimizu, D.J. Smith, Preferential hydration and the exclusion of cosolvents from protein surfaces, J. Chem. Phys. 121 (2004) 1148–1154.
[61] D.R. Canchi, P. Jayasimha, D.C. Rao, G.I. Makhatadze, A.E. Garcia, Molecular mechanism for the preferential exclusion of osmolytes from protein surfaces, Biophys. J. 104 (2013) 189a.
[62] S. Shimizu, Estimating hydration changes upon biomolecular reactions from osmotic stress, high pressure, and preferential hydration experiments, Proc. Natl. Acad. Sci. U. S. A. 101 (2004) 1195–1199.
[63] Q. Zou, B.J. Bennion, V. Daggett, K.P. Murphy, The molecular mechanism of stabilization of proteins by TMAO and its ability to counteract the effects of urea, J. Am. Chem. Soc. 124 (2002) 1192–1202.
[64] D.R. Canchi, A.E. García, Cosolvent effects on protein stability, Annu. Rev. Phys. Chem. 64 (2013) 273–293.
[65] D. Diddens, V. Lesch, A. Heuer, J. Smiatek, Aqueous ionic liquids and their influence on peptide conformations: denaturation and dehydration mechanisms, Phys. Chem. Chem. Phys. 19 (2017) 20430–20440.
[66] J.E.S.J. Reid, E.S. Joshua, A.J. Walker, S. Shimizu, Residual water in ionic liquids: clustered or dissociated? Phys. Chem. Chem. Phys. 17 (2015) 14710–14718.

[67] P.E. Smith, Computer simulation of cosolvent effects on hydrophobic hydration, J. Phys. Chem. B 103 (1999) 525–534.
[68] S. Vijay-Kumar, C.E. Bugg, W.J. Cook, Structure of ubiquitin refined at 1.8 a resolution, J. Mol. Biol. 194 (1987) 531–544.
[69] L. Martínez, R. Andrade, E.G. Birgin, J.M. Martínez, PACKMOL: a package for building initial configurations for molecular dynamics simulations, J. Comput. Chem. 30 (2009) 2157–2164.
[70] J.M. Martínez, L. Martínez, Packing optimization for automated generation of complex system's initial configurations for molecular dynamics and docking, J. Comput. Chem. 24 (2003) 819–825.
[71] D. Van Der Spoel, E. Lindahl, B. Hess, G. Groenhof, A.E. Mark, H.J.C. Berendsen, GROMACS: fast, flexible, and free, J. Comput. Chem. 26 (2005) 1701–1718.
[72] B. Kohnke, R. Thomas Ullmann, C. Kutzner, A. Beckmann, D. Haensel, I. Kabadshow, H. Dachsel, B. Hess, H. Grubmüller, A flexible, GPU - powered fast multipole method for realistic biomolecular simulations in Gromacs, Biophys. J. 112 (2017) 448a.
[73] T. McSherry, A general steepest descent algorithm, IEEE Trans. Aerosp. Electron. Syst. AES-12 (1976) 12–22.
[74] M. Parrinello, A. Rahman, Polymorphic transitions in single crystals: a new molecular dynamics method, J. Appl. Phys. 52 (1981) 7182–7190.
[75] M. Parrinello, A. Rahman, Strain fluctuations and elastic constants, J. Chem. Phys. 76 (1982) 2662–2666.
[76] G. Bussi, D. Donadio, M. Parrinello, Canonical sampling through velocity rescaling, J. Chem. Phys. 126 (2007), 014101.
[77] H.J.C. Berendsen, J.P.M. Postma, W.F. van Gunsteren, A. DiNola, J.R. Haak, Molecular dynamics with coupling to an external bath, J. Chem. Phys. 81 (1984) 3684–3690.
[78] M. Di Pierro, R. Elber, B. Leimkuhler, A stochastic algorithm for the isobaric-isothermal ensemble with Ewald summations for all long range forces, J. Chem. Theory Comput. 11 (2015) 5624–5637.
[79] M.J. Robertson, J. Tirado-Rives, W.L. Jorgensen, Improved peptide and protein torsional energetics with the OPLSAA force field, J. Chem. Theory Comput. 11 (2015) 3499–3509.
[80] W.L. Jorgensen, J. Chandrasekhar, J.D. Madura, R.W. Impey, M.L. Klein, Comparison of simple potential functions for simulating liquid water, J. Chem. Phys. 79 (1983) 926–935.
[81] B. Doherty, X. Zhong, O. Acevedo, Virtual site OPLS force field for Imidazolium-based ionic liquids, J. Phys. Chem. B 122 (2018) 2962–2974.
[82] D. Yalcin, I.D. Welsh, E.L. Matthewman, S.P. Jun, M. Mckeever-Willis, I. Gritcan, T.L. Greaves, C.C. Weber, Structural investigations of molecular solutes within nanostructured ionic liquids, Phys. Chem. Chem. Phys. 22 (2020) 11593–11608.
[83] J. Sánchez-Badillo, M. Gallo, R.A. Guirado-López, J. López-Lemus, Thermodynamic, structural and dynamic properties of ionic liquids [C4mim][CF3COO], [C4mim][Br] in the condensed phase, using molecular simulations, RSC Adv. 9 (2019) 13677–13695.
[84] C. Velez, B. Doherty, O. Acevedo, Accurate Diels-Alder energies and Endo selectivity in ionic liquids using the OPLS-VSIL force field, Int. J. Mol. Sci. 21 (2020) 1190.
[85] U. Kapoor, A. Banerjee, J.K. Shah, Evaluation of the predictive capability of ionic liquid force fields for CH_4, CO_2, NH_3, and SO_2 phase equilibria, Fluid Phase Equilib. 492 (2019) 161–173.
[86] Y. Zhuo, S. Xiao, V. Håkonsen, J. He, Z. Zhang, Anti-icing ionogel surfaces: inhibiting ice nucleation, growth, and adhesion, ACS Materials Letters 2 (2020) 616–623.
[87] J. Bezanson, A. Edelman, S. Karpinski, V.B. Shah, Julia: a fresh approach to numerical computing, SIAM Rev. 59 (2017) 65–98.
[88] W. Humphrey, A. Dalke, K. Schulten, VMD: visual molecular dynamics, J. Mol. Graph. 14 (1996) 33–38.